

# The different faces of 4'-pyrimidinyl functionalized 4,2':6',4''-terpyridines: metal organic assemblies from solution and on Au(111) and Cu(111) surface platforms

Thomas Nijs,<sup>a</sup> Y. Maximilian Klein,<sup>b</sup> S. Fatemeh Mousavi,<sup>a</sup> Aisha Ahsan,<sup>a</sup> Sylwia Nowakowska,<sup>a</sup> Edwin C. Constable,<sup>b</sup> Catherine E. Housecroft<sup>b\*</sup> and Thomas Jung<sup>a,c\*</sup>

<sup>a</sup> Department of Physics, University of Basel, Klingelbergstrasse 82, 4056 Basel, Switzerland

<sup>b</sup> Department of Chemistry, University of Basel, BPR 1096, Mattenstrasse 24a 4058 Basel, Switzerland

<sup>c</sup> Laboratory for Micro- and Nanotechnology, Paul Scherrer Institut, 5232 Villigen, Switzerland.

**KEYWORDS** Coordination network; 4,2':6',4''-terpyridine; copper; scanning tunneling microscopy; on-surface assembly.

**ABSTRACT:** A comparative investigation of crystal growth from solution and on-surface assembly *in vacuo* between copper and three 4'-(2-R-pyrimidin-5-yl)-4,2':6',4''-terpyridines with R = H (**1**), Me (**2**) or Et (**3**) is presented. In solution, ligand **3** combines with copper(II) acetate or copper(I) triflate in MeOH solution to give  $[\text{Cu}_2(\text{OAc})_4(\mathbf{3})]_n$  or  $\{[\text{Cu}(\mathbf{3})(\text{OMe})(\text{MeOH})][\text{CF}_3\text{SO}_3]\text{MeOH}\}_n$ . In  $[\text{Cu}_2(\text{OAc})_4(\mathbf{3})]_n$ , paddle-wheel  $\{\text{Cu}_2(\mu\text{-OAc})_4\}$  nodes direct the assembly of 1D-zigzag chains which pack into 2D sheets. In  $\{[\text{Cu}(\mathbf{3})(\text{OMe})(\text{MeOH})][\text{CF}_3\text{SO}_3]\text{MeOH}\}_n$ , the solvent is both a ligand and generates  $\{\text{Cu}_2(\mu\text{-OMe})_2\}$  units which function as planar 4-connecting nodes to generate a 2D (4,4) net with ligand **3**. On Au(111) or Cu(111) surfaces *in vacuo*, no additional solvent or anions are involved in the assembly. The different substituents in **1**, **2** or **3** allow precise molecular resolution imaging in scanning tunneling microscopy (STM). On Au(111), **1** and **2** assemble into close-packed assemblies, whilst **3** forms a regular porous network. The deposition of Cu ad-atoms results in reorganization leading to ladder-shaped surface metal-organic motifs. These on-surface coordination assemblies are independent of the 4'-substituent in the 4,2':6',4''-tpy and are reproduced on Cu(111) where Cu ad-atoms are available during the deposition and relaxation process at room temperature. Upon annealing at elevated temperatures, the original surface assemblies of **1** and **3** are modified and a transition from ladders into rhomboid structures is observed; for **2**, a further quasi-hexagonal nanoporous network is observed.

## Introduction

One of the most common strategies for supramolecular assembly is predicated upon the interactions of metal centers with ligands.<sup>1</sup> Metallosupramolecular chemistry<sup>2</sup> is concerned with the matching of commensurate metal centers and metal-binding domains. In contrast to single carbon centers which typically exhibit one of three coordination geometries (two-coordinate linear, three-coordinate planar and four-coordinate tetrahedral), metal centers can exhibit coordination numbers from one to at least twelve with all possible geometries.<sup>3</sup> Furthermore, the metal-ligand bond may be labile or kinetically inert,

allowing access to dynamic system.<sup>1</sup> These interactions may be used for the assembly of discrete supramolecular systems or extended one-, two- or three-dimensional assemblies collectively known as coordination polymers.<sup>4</sup> Metal-organic frameworks (MOFs) are well-established three-dimensional examples with wide-ranging applications in catalysis, electrochemistry, host-guest chemistry and fuel cells.<sup>5</sup> Two-dimensional networks can be assembled on an atomically flat substrate, allowing templated host-guest interactions in any pockets in the 2D-lattice. Nevertheless, 3D- and 2D-assemblies differ in the elastic response of the host network and in 2D-networks interaction with the substrate can mediate cooperative effects<sup>6,7,8</sup>

We are interested in the multi-dimensional structural diversity which can be achieved through variation in molecular structure and processing in bulk materials and in monolayers. We also wish to probe the structural consequences of the constraints of assembly processes on surfaces as opposed to those in solution.

Of the 48 isomers of terpyridine, the best known is 2,2':6',2''-terpyridine (2,2':6',2''-tpy, Chart 1) which is a chelating ligand typically presenting a convergent  $N,N,N'$ -donor set to a metal center<sup>9</sup> whereas the less well-investigated 4,2':6',4''-tpy and 3,2':6',3''-tpy (Chart 1) only coordinate to metal centers through the terminal nitrogen donors and present divergent  $N,N'$ -donor sets ideal for the assembly of extended structures with metal nodes.<sup>10,11</sup> Functionality can readily be introduced at the 4'-position<sup>12,13</sup> allowing the construction of ligands with both innocent and non-innocent substituents. Although 4,2':6',4''-tpy ligands are well-established in 1D- and 2D-systems,<sup>9,11</sup> few examples of 3D networks in the absence of peripheral coordination units or co-ligands have been described.<sup>14,15</sup>

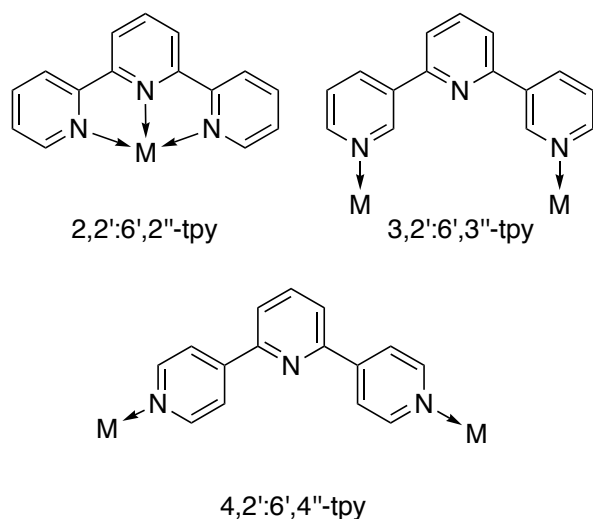


**Chart 1.** Coordination modes of isomeric terpyridines 2,2':6',2''-tpy, 3,2':6',3''-tpy and 4,2':6',4''-tpy. The structural diversity possible with 3,2':6',3''-tpy is greater because of rotation about the interannular C-C bonds.

In networks of 4,2':6',4''-tpy ligands with copper nodes, anions or co-ligands play a critical role in directing the assembly. Reactions of  $\text{CuCN}$  with 4'-aryl-4,2':6',4''-tpy ligands lead to interpenetrated 3D-frameworks with bridging 4,2':6',4''-tpy and cyanido ligands. Increasing the steric demands of the 4'-functionality suppresses the interpenetration.<sup>16</sup> Bridging cyanido linkers also feature in interpenetrated 3D-frameworks found in  $[\text{Cu}_9(4'-(\text{NCC}_6\text{H}_4)-4,2':6',4''\text{-tpy})_{4,5}(\text{CN})_9]_n$  (see Chart 2 for the structure of 4'-( $\text{NCC}_6\text{H}_4$ )-4,2':6',4''-tpy).<sup>17</sup> In both of these networks, the copper(I) centers are 3-coordinate. A carboxylic acid group in the 4'-position of the tpy unit is typically non-innocent,<sup>17,18,19,20</sup> although Xiao and coworkers suggest that the presence of uncoordinated  $-\text{CO}_2\text{H}$

moieties play a role in the assembly of an unusual 2D $\rightarrow$ 2D polythreaded network.<sup>21</sup> The ligand 4'-(4-pyridyl)-4,2':6',4''-tpy (Chart 2) is well-explored and coordination to copper(I) through both the 4,2':6',4''-tpy and pendant pyridyl units leads to a 3D-network with 4-fold interpenetration; in this case nitrate counter-ions and MeOH solvent molecules are accommodated along channels in the structure.<sup>22</sup> Reactions of copper(II) acetate with 4'-aryl-4,2':6',4''-tps (aryl = biphenyl,<sup>23</sup> 2',3',4',5',6'-pentafluorobiphenyl,<sup>23</sup> phenyl,<sup>24</sup> 4-dimethylaminophenyl<sup>24</sup>) lead to 1D-coordination polymers incorporating paddle-wheel  $\{\text{Cu}_2(\mu\text{-OAc})_4\}$ -nodes connected by bridging 4,2':6',4''-tpy domains.

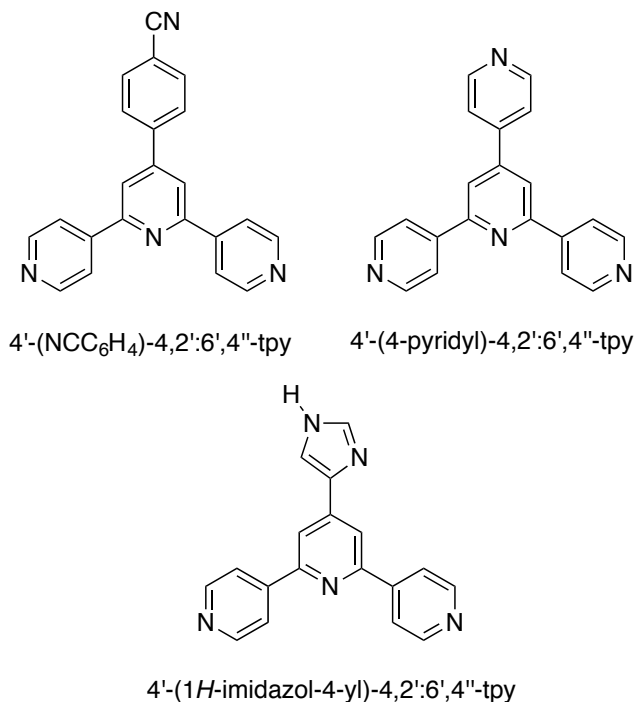


**Chart 2.** Structures of selected 4'-functionalized 4,2':6',4''-tpy ligands.

We are interested in 4,2':6',4''-tpy building blocks functionalized in the 4'-position with  $N$ -heterocycles other than pyridine, and focus upon copper as the metal-node for the assembly of multidimensional networks. The originality of our approach is to combine studies of crystal growth under ambient solution conditions with on-surface deposition on Au(111) and Cu(111) substrates under ultrahigh vacuum (UHV) to investigate the interactions of these ligands with metal centers. This strategy allows us to probe the assembly process with a constant pairing of metal and ligand with and without constraints imposed by a surface architecture. In solution, the oxidation state of the metal-node ( $\text{Cu}^+$  or  $\text{Cu}^{2+}$ ) is defined and counter-ions are required for charge neutrality; furthermore, crystallization typically results in incorporation of lattice solvent molecules. In contrast,

on-surface assemblies initiated by copper ad-atoms yield structures free from counter-ions and solvent molecules. Both 4'-(1*H*-imidazol-4-yl)-4,2':6',4''-tpy (Chart 2) and 4'-(pyrimidin-5-yl)-4,2':6',4''-tpy (**1**, Chart 3) are attractive building blocks containing both a divergent V-shaped tecton and a functionality with potential for further coordination although their coordination chemistry has been little explored. Each might direct the assembly of 1D chains or 2D-networks depending upon the coordinative innocence or non-innocence of the pendant heterocyclic substituent. 4'-(1*H*-Imidazol-4-yl)-4,2':6',4''-tpy forms hydrogen-bonded domains on an Au(III) surface and the addition of copper ad-atoms results in reorganization into a 2D-coordination network; the *N*-donors of both the 4,2':6',4''-tpy and imidazolyl units are bonded to copper.<sup>25</sup> In the only example of a coordination assembly involving 4'-(1*H*-imidazol-4-yl)-4,2':6',4''-tpy under solution conditions, the imidazolyl unit is uncoordinated.<sup>26</sup> We have also shown that **1** and its 2-methyl substituted derivative **2** bind zinc(II) selectively through the 4,2':6',4''-tpy domain.<sup>27</sup> In contrast, the pendant pyrimidinyl domains in [Ru(**4**)<sub>2</sub>]<sup>2+</sup> (Chart 3) bind copper(II) to generate a 2D-network.<sup>28</sup> In the present work, we report the coordination behavior of pyrimidinyl-functionalized ligands **1–3** (Chart 3) with copper with an emphasis on contrasting the coordination behaviour in solution with on-surface interactions of these ligands with copper ad-atoms. The surface-immobilized networks can be tuned by varying the length of any 2-substituent attached to the pyrimidine ring or through external stimulus in the form of annealing.

## Experimental section

Experimental details and crystallographic data are given in the electronic supporting information.

## Results and discussion

### Synthesis and characterization of compound **3**

We have previously reported ligands **1** and **2**,<sup>27</sup> and compound **3** was synthesized in an analogous manner using the one-pot methodology of Hanan.<sup>13</sup> The electrospray mass spectrum of **3** showed a base peak at *m/z* 340.23 corresponding to [M+H]<sup>+</sup>. The <sup>1</sup>H and <sup>13</sup>C NMR spectra of **3** (Figs. S1 and S2) were assigned by COSY, NOESY, HMQC and HMBC methods and were in accord with the structure shown in Chart 3.

### Assembly in solution of a 1D-coordination polymer and a 2D-net

Reactions of ligands **1**, **2** or **3** with copper(II) acetate or copper(I) triflate were investigated by room temperature crystal growth experiments by layering an MeOH solution of each copper salt over a CHCl<sub>3</sub> solution of the ligand. X-ray quality crystals [Cu<sub>2</sub>(OAc)<sub>4</sub>(**3**)<sub>n</sub> and {[Cu(**3**)(OMe)(MeOH)][CF<sub>3</sub>SO<sub>3</sub>]<sup>-</sup>MeOH]<sub>n</sub> were obtained after 1–2 weeks. Their structures illustrate the roles that

the counterion (acetate or triflate) and solvent play in directing the coordination assembly.

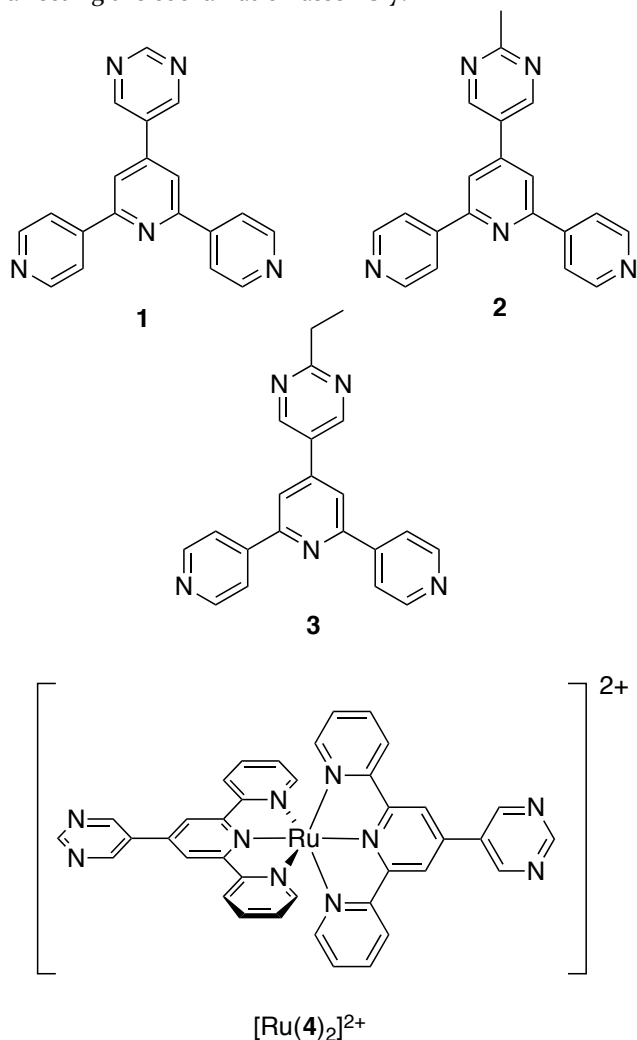


**Chart 3.** Structures of ligands **1–3** and of the pyrimidinyl-functionalized complex [Ru(**4**)<sub>2</sub>]<sup>2+</sup>.

[Cu<sub>2</sub>(OAc)<sub>4</sub>(**3**)<sub>n</sub> comprises paddle-wheel {Cu<sub>2</sub>(μ-OAc)<sub>4</sub>} units linked by molecules of **3** which coordinate through the outer N atoms of the 4,2':6',4''-tpy unit (Fig. S3). The coordination polymer crystallizes in the monoclinic *C*<sub>2</sub>/*c* space group and the asymmetric unit contains one Cu(OAc)<sub>2</sub> unit and half of one ligand **3**. The second half of the paddle-wheel motif is generated by inversion, and the second half of the 4,2':6',4''-tpy unit by 2-fold rotation. The 2-ethylpyrimidinyl unit is disordered with one complete half-occupancy ring and ethyl group in the asymmetric unit (as depicted in Fig S3) and the second half-occupancy ring generated by rotation about a 2-fold axis. Selected bond parameters describing coordination at atom Cu1 are shown in the caption to Fig. S3. The structure propagates in a zigzag chain (Fig. 1a) and is related to a series of coordination polymers containing 4'-substituted 4,2':6',4''-tpys and supported by {Cu<sub>2</sub>(μ-OAc)<sub>4</sub>} or {Zn<sub>2</sub>(μ-OAc)<sub>4</sub>} paddle-wheel nodes.<sup>23,29,30,31,32,33,34</sup>

The zigzag chains pack into 2D-sheets with the 2-ethylpyrimidinyl unit nestling into the V-shaped cavity offered by the 4,2':6',4''-tpy unit of an adjacent chain (Fig. 1b). Finally, 2D-sheets are associated through  $\pi$ -stacking interactions between 4,2':6',4''-tpy units in different chains (Fig. 1c). Pairs of pyridine rings containing Ni<sup>i</sup>/N<sub>2</sub> in one 4,2':6',4''-tpy and Ni<sup>iii</sup>/N<sub>2</sub><sup>iv</sup> in an adjacent 4,2':6',4''-tpy (symmetry codes: i = 1-x, y, 3/2-z; iii = x, 1-y, 1/2+z; iv = 1-x, 1-y, 2-z) are related by inversion and adopt an offset orientation (Fig. 1c) typical of an efficient face-to-face  $\pi$ -stack.<sup>35</sup> The distance between the planes of pairs of stacked pyridine rings is 3.32 Å and the inter-centroid separation is 3.64 Å. The assembly of chains in [Cu<sub>2</sub>(OAc)<sub>4</sub>(**3**)<sub>n</sub>] is predicated upon paddle-wheel {Cu<sub>2</sub>( $\mu$ -OAc)<sub>4</sub>} units acting as 2-connecting nodes,<sup>9,36,37</sup> and in [Cu<sub>2</sub>(OAc)<sub>4</sub>(**3**)<sub>n</sub>], the acetate anions play a crucial role as bridging ligands in the {Cu<sub>2</sub>( $\mu$ -OAc)<sub>4</sub>} nodes contributing fundamentally to the assembly process.

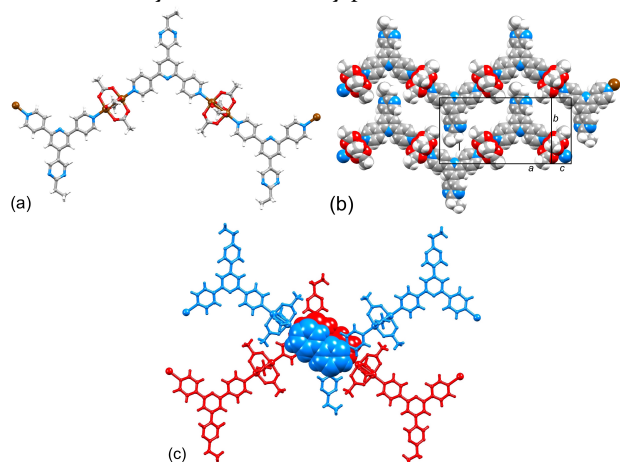


**Fig. 1.** (a) Part of one zigzag chain in [Cu<sub>2</sub>(OAc)<sub>4</sub>(**3**)<sub>n</sub>]. (b) Packing of adjacent chains to form a 2D-sheet. (c)  $\pi$ -Stacking interactions between 4,2':6',4''-tpy domains in chains in adjacent sheets.

Layering a MeOH solution of copper(I) triflate over a CHCl<sub>3</sub> solution of **3** resulted in X-ray quality blue needles. The color suggested aerial oxidation to copper(II) as confirmed by the single crystal structure of {[Cu(**3**)(OMe)(MeOH)][CF<sub>3</sub>SO<sub>3</sub>]MeOH}<sub>n</sub>. The compound crystallizes in the monoclinic space group *P*2<sub>1</sub>/*n* and Fig. S4 depicts the repeat unit in the extended structure. Ligand **3** coordinates to Cu<sup>i</sup> and the symmetry-generated Cu<sup>i</sup> (see Fig. S4 caption) through the outer two nitrogens N<sub>1</sub> and N<sub>3</sub>. Atoms N<sub>2</sub>, N<sub>4</sub> and N<sub>5</sub> in the central pyridine and pyrimidine rings, respectively, are non-coordinated. Atom Cu<sup>i</sup> is in a square-based pyramidal environment ( $\tau = 0.20$ )<sup>38</sup> bound in two, mutually *cis*, basal sites to N<sub>3</sub> and N<sub>3</sub><sup>iii</sup> of two different ligands **3**. The remaining basal sites are occupied by methoxy ligands which support a {Cu<sub>2</sub>( $\mu$ -OMe)<sub>2</sub>} unit. A MeOH molecule bound through O<sub>2</sub> (Fig. S4) occupies the axial site of Cu<sup>i</sup>. The {Cu<sub>2</sub>( $\mu$ -OMe)<sub>2</sub>} units act as planar, 4-connecting nodes linked by the 4,2':6',4''-tpy domains of **3** to generate a 2D (4,4) net. A TOPOS<sup>39</sup> representation is shown in Fig. 2a with the molecular network overlaid. Within the 4,2':6',4''-tpy unit,

adjacent pyridine rings are twisted 14.9 and 30.7°, with respect to one another. The plane of the pyrimidine ring is twisted only 7.0° with respect to the pyridine ring containing N<sub>2</sub> (Fig. S4). This near planarity is associated with face-to-face  $\pi$ -stacking of pyrimidin-5-ylpyridine units in adjacent ligands (Fig. 2b). The stacked units are related by inversion, and adopt an optimal offset arrangement.<sup>35</sup> The separation of the least squares planes through the pyrimidin-5-ylpyridine units containing N<sub>2</sub>/N<sub>4</sub>/N<sub>5</sub> and N<sub>2</sub><sup>iv</sup>/N<sub>4</sub><sup>iv</sup>/N<sub>5</sub><sup>iv</sup> is 3.48 Å and the pyridine...pyrimidine centroid-to-centroid distance is 3.60 Å. The interactions lock the ligands into a compact 2D-sheet, the cavities in which (Fig. 2b) are occupied by triflate anions which exhibit short F...H and O...H contacts within the sheet. There are no  $\pi$ -stacking contacts between 2D-sheets. In the assembly of {[Cu(**3**)(OMe)(MeOH)][CF<sub>3</sub>SO<sub>3</sub>]MeOH}<sub>n</sub>, the choice of methanol as solvent plays a critical role, facilitating the formation of {Cu<sub>2</sub>( $\mu$ -OMe)<sub>2</sub>} units which are the 4-connecting nodes that direct the assembly of the 2D-sheet.

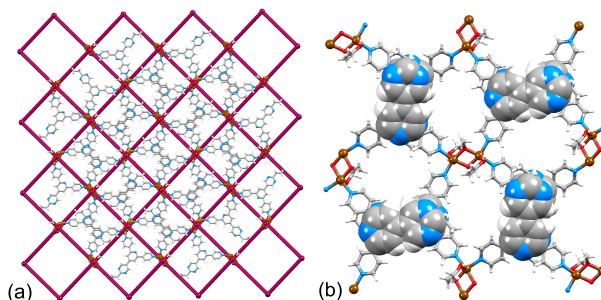


**Fig. 2.** The 2D-network in {[Cu(**3**)(OMe)(MeOH)][CF<sub>3</sub>SO<sub>3</sub>]MeOH}<sub>n</sub>: (a) TOPOS<sup>39</sup> representation with overlaid structure of part of one (4,4) net, and (b) part of one 2D-sheet showing the  $\pi$ -stacking interactions between pyrimidin-5-ylpyridine units in adjacent ligands **3**.

### On-surface assemblies

The solution-based assemblies described above highlight not only the critical roles of solvent and counterions but also emphasizes the expected<sup>27</sup> coordination of **3** through only the outer *N*-atoms of the 4,2':6',4''-tpy domain. Solution-based coordination assemblies using 4'-(1*H*-imidazol-4-yl)-4,2':6',4''-tpy (Chart 2) as the organic linker involve only the outer *N*-donors of the 4,2':6',4''-tpy unit<sup>26</sup> but in contrast, the *N*-donors of the 4,2':6',4''-tpy and imidazolyl units are involved in binding copper adatoms when the latter are added to an assembly of the ligand on an Au(111) surface.<sup>25</sup> We now demonstrate that this switch in coordination behavior is also observed for ligands **1-3**. Compounds **1-3**, differing only by the presence of an H, Me or Et 2-substituent on the pyrimidin-5-yl functionality (Chart 3 and Fig. 3) were deposited under UHV conditions by thermal sublimation. X-ray photoelectron spectroscopy (XPS) data were used to confirm that the compounds were deposited without chemical change by analyzing the relative ratios of the (deconvoluted) peaks (see Fig. S6). Molecule **1** defines an equilateral triangle whereas in **2** and **3**, the alkyl substituents act

as an ‘imaging group’ in the scanning tunneling microscope (STM) micrographs shown in Figs. 3 and S7. Thus, as the substituent increases in size, it is possible to visualize molecular orientation.

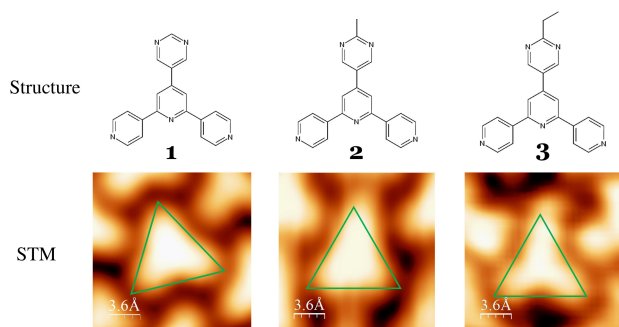


**Fig. 3.** Structures and corresponding STM micrographs of compounds **1, 2** and **3** on a Au(111) substrate taken at 5 K with clearly distinguishable alkyl vertices allowing assignment of orientation. An equilateral triangle has been superimposed onto each image to guide the eye towards the different STM contrasts for the molecules. An enlarged version of the figure is given in Fig. S7.

When deposited on the inert surface of Au(111), **1** and **2** arrange in extended close-packed phases (Figs. 4 and S8, top) attributed to the symmetry of the molecules, allowing for high packing densities in 2D-arrangements. Differently oriented domains are separated by two types of boundaries, depending on the relative orientations of two domains (zipper-like or avoiding). In addition to weak non-classical C-H...N hydrogen-bond interactions,<sup>40</sup> attractive dipole forces are balanced by repulsive H...H interactions. The larger, and less symmetrical, ethyl substituent in **3** increases the ‘footprint’ of the molecule and causes a looser 2D-assembly while maintaining the principal assembly motifs. The ethyl groups are located in the so-formed cavity (Fig. 4, top right) giving rise to highly-structured alternating lines in three principal directions. This space-optimizing is reflected in the unit-cells of the assemblies, marked in green in the insets in Fig. 4. The unit cell of **1** is  $1 \times 1 \text{ nm} = 1 \text{ nm}^2$ , of **2** is  $1 \times 1.25 \text{ nm} = 1.25 \text{ nm}^2$ , and of **3** is  $2.05 \times 2.05 \text{ nm} = 4.20 \text{ nm}^2$  consistent with going from a pyrimidinyl to 2-methylpyrimidinyl to 2-ethylpyrimidinyl substituent. The unit cells of the adlayer exhibit a  $60^\circ/120^\circ$  symmetry (see model Fig. 4, as well as the insets) which is broken by the superposition with the Au(111) $22 \times \sqrt{3}$  reconstruction (*vide infra*).

The *in-situ* addition of Cu-ad-atoms from a thermal evaporation source to the molecular assemblies of **1, 2** or **3** on Au(111) at room temperature results, in each case, in the formation of long, straight ladder-like chains. For **3** this is shown in Fig. 4 and a comparison of the assemblies for all three ligands is shown in Fig. S9, top. To investigate the origin of the re-organization of the on-surface assembly, XPS data were acquired before and after the addition of copper atoms. The peak at 398.9 eV marked in blue in Figs. 4 and S8 arises from the uncoor-

inated N-atoms. As we have previously shown,<sup>25</sup> the N-atom of the central ring of the 4,2':6',4''-tpy unit does not coordinate, confirmed by the retention of the peak at 398.9 eV after Cu ad-atoms have been supplied. The XPS spectra are consistent with coordination to copper of both the outer N-donors of the 4,2':6',4''-tpy unit and the two pyrimidinyl N atoms, with the ratio of the new peak at 399.6 eV (shown in red in Fig. 4 or Fig. S10) to the peak at 398.9 eV being 4 : 1.

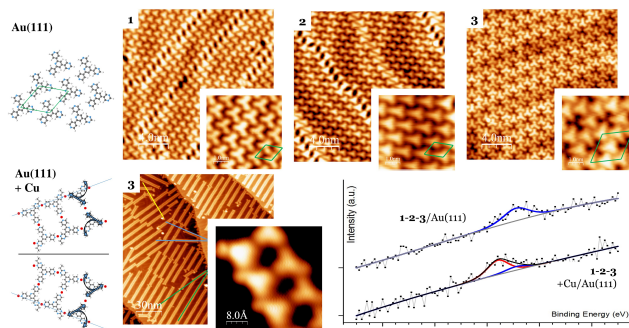


**Fig. 4.** Molecules on Au(111) substrate. Top row: before Cu-coordination, **1** and **2** assemble into a close-packed layer, whereas **3** forms a regular porous vacancy pattern; each  $5 \times 5 \text{ nm}$  inset shows the unit cell in green to emphasize the influence of the substituent on the 2D assembly. Bottom left: after Cu-coordination, 1D ladder-like structures assemble. The expansion shows that the ethyl groups point to the outside of the ladder. Chains are oriented in six directions, five of which are shown and indicated as blue, green and yellow lines. Bottom right, XPS data showing the chemical change in the N environment, indicating metal coordination of the outer N (red line), while the inner pyridine-ring N of the tpy unit remains unchanged (blue line). An enlarged version of the figure is given in Fig. S8.

The assembly of the ladder-like arrays arises from the rearrangement of the molecules to optimize coordination to the Cu-ad-atoms, and leads to 1D coordination double-chains (see model Fig. 5 for more detail). The assemblies appear to be robust since the ladders remain straight and periodic across the complex domain pattern of the Au(111) $22 \times \sqrt{3}$  reconstruction. This well known surface reconstruction occurs due to a reorganization of the top layer of the gold substrate under strain, resulting in herringbone shaped striped domains with different stacking, hcp vs. fcc of the top layer Au atoms on the fcc crystal below. The domain walls of the reconstructed Au top layer atoms in between these domains are slightly elevated and visualized in STM as a herringbone pattern.<sup>41,42</sup> The structural models in Figs. 4 and S8 reflect what can be seen in the STM data after identification of the substituents of **2** and **3** which point to the outside of the ladders and are most clearly seen in the enlargement of the STM image of **3**. Each unit cell involves three Cu-ad-atoms; in other words, three of the four coordinated N-atoms share a Cu ad-atom with an N-atom of a neighboring molecule (marked as red dots). Additionally, due to the orientation of the molecule within the

ladder, both left- and right-handed chiralities are present in the three directions related by  $120^\circ$  (see yellow, blue and green lines in the middle image of the bottom row in Fig. 4; only five of the six directions are within the frame shown). The angle between ladders of opposite chiralities formed upon adsorption on the substrate depends on the molecular building block and is  $20^\circ$  for **3** and  $38^\circ$  for **2**. There is no evidence from either XPS or the STM analysis that Au-ad-atoms from the substrate are involved in the formation of similar ladder-like assemblies.<sup>43</sup>

Deposition of ligands **1–3** was also carried out on a Cu(111) substrate held at room temperature (see Fig. S11 for XPS multilayer result) which provides Cu-ad-atoms for coordination from the surface during preparation.<sup>44,45,46</sup> Even though the change of substrate from Au(111) to Cu(111) involves a change in lattice constant, we observe a remarkable consistency in the morphology of both assemblies (Figs. 5 and S12 versus Fig. S9). The appearance of the same ladder-like assemblies testifies to this being a robust motif and any differences between Cu(111) and Au(111) surfaces are within the error of the measurements. The chain width coincidentally is 2.3 nm ( $23 \text{ \AA}$ ) on both substrates which is equivalent to  $8 \times 2.88 \text{ \AA}$  (gold lattice constant) or  $9 \times 2.56 \text{ \AA}$  (copper lattice constant). The lack of dependence of the core assembly on the substituent is remarkable. As observed on Au(111), the ladders on Cu(111) also reveal their chirality, although in this case, all three functionalities (with **1**, **2** or **3**) have the same  $13 \pm 1^\circ$  chirality angle. All molecules in one strand are oriented in one direction, while all molecules from the other strand point in the opposite direction. No achiral ladders were observed.

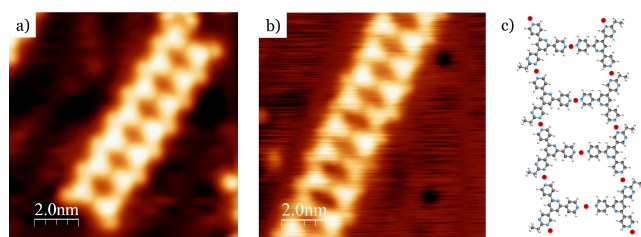


**Fig. 5.** Comparison of ladders of **3** on a) Au(111)+Cu ad-atoms, and b) Cu(111). The assemblies are also similar for **1** and **2** (see Fig. S7 for full matrix). (c) Model of part of one chain showing the ethyl substituent pointing to the outside of the ladder. An enlarged version of the figure is given in Fig. S12.

As displayed in Fig. S13, ladders can reach remarkable lengths of over 125 nm. The discontinuities visible in the chains (e.g. Figs. 6 and S14, top left) are attributed to a jump in the registry in a lateral direction of one row on the Cu(111) substrate. The 2D-assemblies of ladders are stable up to room temperature, but structural perturbation was achieved by annealing on the Cu(111) substrate. In a first stage, the ladders were transformed to tetramers (20 minutes at  $240^\circ\text{C}$ , Fig. 6b), and after further annealing for 20 minutes at  $290^\circ\text{C}$ , hexagonal motifs were formed (Fig. 6c). These hexagonal assemblies could

also be obtained in a single annealing step of 30 minutes at  $240^\circ\text{C}$ .

The tetramers exhibit three distinct orientations, related by  $120^\circ$  rotations (see the three tetramers highlighted in green in Figs. 6b and S14b). For the rhombi, the internal angles are consistently  $80/100^\circ$ , due to the mismatch of square assemblies on a hexagonally oriented substrate. As with the ladder assemblies, the structure is not dependent on the substituents in **1**, **2** and **3**, which are directed outside the assembly motif (rhombus side length of  $2.3 \text{ nm} \pm 0.1 \text{ nm}$ ; see Fig. S15 for a detailed comparison). A similar result is observed when directly depositing **1**, **2** or **3** on a hot Cu(111) substrate, omitting the ladder assembly. Due to the availability of Cu ad-atoms at higher temperatures,<sup>47</sup> there is a smaller tendency for the organic molecules to share the Cu ad-atoms with their neighbors. This results in a preference for discrete tetramers over ladders. Per tetrameric motif, four Cu ad-atoms are involved in bonding forming a [4+4] metallomacrocylic unit. This results in two shared ad-atoms per molecule in comparison to three for the ladders (see Fig. S15 for a detailed model).

Unexpectedly, further annealing of the tetramers on Cu(111) with ligand **2** results in a further rearrangement into the nanoporous network seen in Figs. 6c and S14c. Within the series of molecules **1–3**, the most compact packing is obtained with the methyl substituent (Figs. 6 and S14, bottom row); in the analogous assembly formed with **1**, repulsive interactions involving  $\text{H}_2$  would destabilize this arrangement, whereas with **3** the ethyl has too great a steric demand.<sup>48,49</sup> It is remarkable, how small changes in the alkyl substituent result in such dramatic effects on the surface assembly. The nanoporous assembly of **2** (Fig. 6c) is present in both chiral forms (see Fig. S16).

Temperature dependent XPS analysis was carried out, revealing neither an annealing dependency of the on-surface assembly (see first column of Fig. S17; in line with the result of **1**, **2**, **3** on Au(111) + Cu ad-atoms where full coordination already takes place at room temperature) nor compound dependency (see right column of Fig. S17 for **2** vs. **3** comparison; for all compounds N 1s peaks are at  $\sim 398.6$  and  $399.7 (\pm 0.2) \text{ eV}$ ). This result shows that the different behavior of **1**, **2** and **3** is not based on differing chemical reactivity, but rather on the steric demand of the substituents. Tables S1 and S2 give a detailed XPS summary.

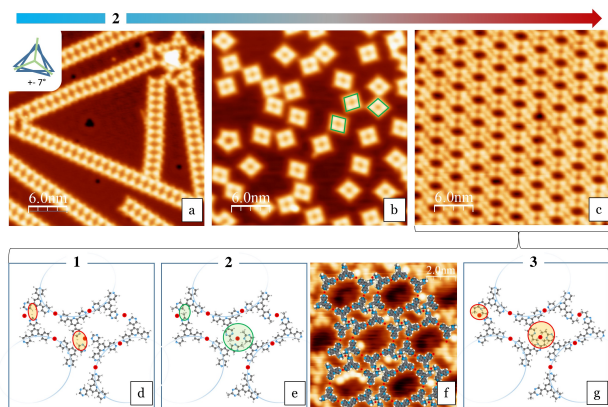


**Fig. 6.** Sequential surface rearrangement. Top: Annealing sequence of **2** (RT, 20 minutes @ 240 °C, additional 20 minutes @ 290 °C). Ladders and tetramers are found for all three molecules **1–3**, but only **2** forms the porous network. Bottom: Closer examination of quasi-hexagon nanoporous network formation. d) R = H: high repulsive H...H interactions. e) R = Me: the ideal case, where in-plane hydrogen is positioned in-between tetrahedral oriented neighbors. f) Space filling models of **2** superimposed on a high-quality STM micrograph (base of the models) (recorded with Xe functionalized tip, with single Xe atoms visible as bright protrusions). g) R = Et: repulsion between the Et groups leads to less efficient packing. For simplicity, non-relevant Cu-ad-atoms have been omitted. An enlarged version of the figure is given in Fig. S14.

## Conclusions

In conclusion, we have adopted an unconventional approach to metal-organic architectures by investigating how a common pair of ligand and metal responds to assembly in solution under ambient conditions or on a Au(III) or Cu(III) surface under UHV conditions. In solution, ligand **3** combines with copper(II) acetate or copper(I) triflate in MeOH to yield single crystals of, respectively,  $[\text{Cu}_2(\text{OAc})_4(\mathbf{3})]_n$  or  $\{[\text{Cu}(\mathbf{3})(\text{OMe})(\text{MeOH})][\text{CF}_3\text{SO}_3]\text{MeOH}\}_n$ . In the former, the acetate anions are critical to the formation of paddle-wheel  $\{\text{Cu}_2(\mu\text{-OAc})_4\}$  units which act as linear nodes and direct the assembly of 1D-zigzag chains. In the latter, the methanol solvent is involved in the assembly of  $\{\text{Cu}_2(\mu\text{-OMe})_2\}$  units which act as planar, 4-connecting nodes connected by ligands **3** to generate a 2D (4,4) net. The roles of solvent and counter-anion are negated by moving from solution to surface assemblies under vacuum. The different R groups in **1**, **2** or **3** have been used as an imaging tool for STM. The difference in the substitution is visible in the close-packed phase on Au(III). After deposition of Cu ad-atoms, regular (ladder-shaped) surface metal-organic motifs assemble on the Au(III) surface, and in all cases exhibit the same backbone structure, indicating the assembly is not influenced by the substituent. The ladder structure also assembles on Cu(III) where Cu ad-atoms are available during the deposition and subsequent relaxation process at room temperature. With progressively increasing annealing temperature, the original surface assemblies are modified and undergo a transition

from ladders into rhomboid structures, and for ligand **2**, a quasi-hexagonal nanoporous network is observed.

Although both the assembly in solution and the solvent-free coordination assembly in vacuum provide coordination assemblies featuring planar layers, there is an important difference. The Cu coordination center in the case of the solution assembly follows the rules of coordination chemistry while the substrate-supported Cu coordination centers also show other more planar motifs, stabilized by the coordinated metal atom interacting with the underlying substrate. It is also interesting to note that this ‘surface supported’ Cu coordination does not appear to depend on whether Au(III) or Cu(III) substrates are used. The inclusion of counter-ions and solvent molecules in the lattice determine that bulk crystalline material and surface assemblies differ in their microstructures, motivating further in depth investigations. It is remarkable, however, that the general principles and algorithms determining the structures of solution grown crystalline material can be extended to surface assemblies.

## ASSOCIATED CONTENT

### Supporting Information

Experimental details; NMR spectra; ORTEP-style figures; powder diffraction data; enlarged versions of manuscript figures and additional STM images; XPS analysis. The Supporting Information is available free of charge on the ACS Publications website.

## AUTHOR INFORMATION

### Corresponding Author

\*C.E. Housecroft: catherine.housecroft@unibas.ch; T.A. Jung: thomas.jung@psi.ch

### Author Contributions

The manuscript was written through contributions of all authors. All authors have given approval to the final version of the manuscript.

### Funding Sources

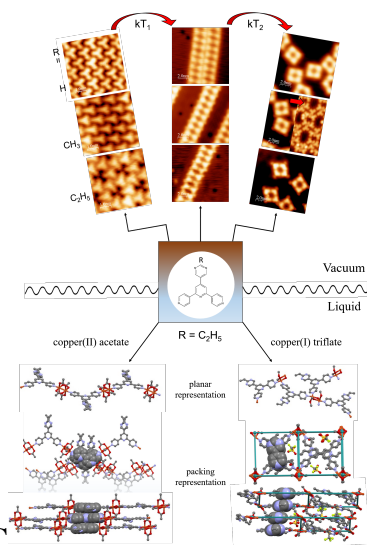
We thank the Swiss National Science Foundation (grant numbers 200020\_162631, 200020-149713 and 206021-121461), the Swiss Nanoscience Institute P1203, the Swiss Commission for Technology and Innovation (CTI, 16465.1 PFNM-NM) and the Swiss Government Excellence Scholarship Program for Foreign Scholars, as well as and the University of Basel for financial support.

## ACKNOWLEDGMENTS

Dr Markus Neuburger (University of Basel) is thanked for assistance with single-crystal structure determinations, Aneliia Wäckerlin (University of Basel) for initial assistance and discussions, Mariah O’Doherty (Trinity College, Dublin) for assisting with the STM experiments and for helpful discussions, and Marco Martina and Matthes Senn (University of Basel) for technical support.

## REFERENCES

- 1 Constable, E.C. *Adv. Inorg. Chem.*, **2018**, in press.
- 2 Constable, E.C. *Chem. Ind.* **1994**, 56.
- 3 Housecroft, C.E.; Sharpe, A.G. *Inorganic Chemistry*, 4th ed., Pearson Education Ltd., Harlow, **2012**.
- 4 Batten, S.R.; Neville, S.M.; Turner, D.R. *Coordination Polymers: Design, Analysis and Application*, RSC Publishing, Cambridge, **2009**.
- 5 See for example: Kang, Z.; Fan, L.; Sun, S. *J. Mater. Chem. A* **2017**, *5*, 10073; Huang, Y.-B.; Liang, J.; Wang, X.-S.; Cao, R. *Chem. Soc. Rev.* **2017**, *46*, 126; Canivet, J.; Vandichel, M.; Farrusseng, D. *Dalton Trans.* **2016**, *45*, 4090; Liu J.; Woll C. *Chem. Soc. Rev.* **2017**, *46*, 5730; Li, B.; Wen, H.-M.; Cui, Y.; Zhou, W.; Qian, G.; Chen, B. *Adv. Mater.* **2016**, *28*, 8819; Furukawa, H.; Cordova, K.E.; O'Keeffe, M.; Yaghi, O.M. *Science*, **2013**, *341*, 974; Schoedel, A.; Li, M.; Li, D.; O'Keeffe, M.; Yaghi, O.M. *Chem. Rev.* **2016**, *116*, 12466.
- 6 Spillmann, H.; Kiebele, A.; Stöhr, M.; Jung, T.A.; Bonifazi, D.; Cheng, F.; Diederich, F. *Adv. Mater.* **2006**, *18*, 275.
- 7 Nowakowska, S.; Wäckerlin, A.; Kawai, S.; Ivas, T.; Nowakowski, J.; Fatayer, S.; Wäckerlin, C.; Nijs, T.; Meyer, E.; Björk, J.; Stöhr, M.; Gade, L.H.; Jung, T.A. *Nature Commun.* **2015**, *6*, article: 6071.
- 8 Nowakowska, S.; Wäckerlin, A.; Piquero-Zulaica, I.; Nowakowski, J.; Kawai, S.; Wäckerlin, C.; Matena, M.; Nijs, T.; Fatayer, S.; Popova, O.; Ahsan, A.; Mousavi, S.F.; Ivas, T.; Meyer, E.; Stöhr, M.; Ortega, J.E.; Björk, J.; Gade, L.H.; Lobo-Checa, J.; Jung, T.A. *Small*, **2016**, *12*, 3757.
- 9 Constable E.C. *Chem. Soc. Rev.*, 2007, **36**, 246.
- 10 Housecroft, C. E. *Dalton Trans.* **2014**, *43*, 6594.
- 11 Housecroft, C. E. *CrystEngComm* **2015**, *17*, 7461.
- 12 Kröhnke, F. *Synthesis*, **1976**, 1.
- 13 Wang J.; Hanan, G.S. *Synlett* **2005**, 1251.
- 14 Klein, Y.M.; Prescimone, A.; Pitak, M.B.; Coles, S.J.; Constable, E.C.; Housecroft, C.E. *CrystEngComm* **2016**, *18*, 4704.
- 15 Yin, Z.; Zhang, S.; Zheng, S.; Golen, J.A.; Rheingold A.L.; Zhang, G. *Polyhedron* **2015**, *101*, 139.
- 16 Li, X.-Z.; Zhou, X.-P.; Li, D.; Yin, Y.-G. *CrystEngComm* **2011**, *13*, 6759.
- 17 Xi, Y.; Wei, W.; Xu, Y.; Huang, X.; Zhang, F.; Hu, C. *Cryst. Growth Des.* **2015**, *15*, 2695.
- 18 Yuan, F.; Xie J.; Hu, H.-M.; Yuan, C.-M.; Xu, B.; Yang, M.-L.; Ding F.-X.; G.-L. Xue, *CrystEngComm* **2013**, *15*, 1460.
- 19 Gong, Y.; Zhang, M.M.; Zhang, P.; Shi, H.F.; Jiang, P.G.; Lin, J.H. *CrystEngComm* **2014**, *16*, 9882.
- 20 Yuan, F.; Zhu, Q.; Hu, H.-M.; Xie, J.; Xu, B.; Yuan, C.-M.; Yang, M.-L.; Dong, F.-X.; Xue, G.-L. *Inorg. Chim. Acta* **2013**, *397*, 117.
- 21 Yang, J.; Yan, S.-W.; Wang, X.; Xiao, D.-R.; Zhang, H.-Y.; Chi, X.-L.; Zhang, J.-L.; Wang, E. *Inorg. Chem. Commun.* **2013**, *38*, 100.
- 22 Chen, Y.-Q.; Li, G.-R.; Cheng, Z.; Qu, Y.-K.; Zhang, Y.-H.; Bu, X.-H. *Chem. Sci.* **2013**, *4*, 3678.
- 23 Constable, E.C.; Housecroft, C.E.; Neuburger, M.; Schönle, J.; Vujovic, S.; Zampese, J. A. *Polyhedron* **2013**, *60*, 120.
- 24 Li, L.; Zhang, Y.Z.; Yang, C.; Liu, E.; Golen, J.A.; Zhang, G. *Polyhedron* **2016**, *115*, 115.
- 25 Nijs, T.; Malzner, F.J.; Fatayer, S.; Wäckerlin, A.; Nowakowska, S.; Constable, E.C.; Housecroft, C.E.; Jung, T.A. *Chem. Commun.* **2015**, *51*, 12297.
- 26 Constable, E.C.; Housecroft, C.E.; Neuburger, M.; Vujovic, S.; Zampese, J.A.; Zhang, G. *CrystEngComm* **2012**, *14*, 3554.
- 27 Klein, Y.M.; Constable, E.C.; Housecroft, C.E.; Zampese, J.A. *Polyhedron* **2014**, *81*, 98.
- 28 Beves, J.E.; Constable, E.C.; Decurtins, S.; Dunphy, E.L.; Housecroft, C.E.; Keene, T.D.; Neuburger, M.; Schaffner, S. *CrystEngComm* **2008**, *10*, 986.
- 29 Constable, E.C.; Zhang, G.; Coronado, E.; Housecroft, C. E.; Neuburger, M. *CrystEngComm* **2010**, *12*, 2139.
- 30 Constable, E.C.; Zhang, G.; Housecroft, C.E.; Neuburger, M.; Zampese, J.A. *CrystEngComm* **2010**, *12*, 2146.
- 31 Constable, E.C.; Housecroft, C.E.; Kopecky, P.; Neuburger, M.; Zampese, J.A.; Zhang, G. *CrystEngComm* **2012**, *14*, 446.
- 32 Constable, E.C.; Housecroft, C.E.; Vujovic, S.; Zampese, J.A.; Crochet, A.; Batten, S.R. *CrystEngComm* **2013**, *15*, 10068.
- 33 Klein, Y.M.; Constable, E. C.; Housecroft, C. E.; Zampese, J. A.; Crochet, A. *CrystEngComm* **2014**, *16*, 9915.
- 34 Zhang, G.; Jia, Y.-X.; Chen, W.; Lo, W.-F.; Brathwaite, N.; Golan, J.A.; Rheingold, A.L. *RSC Adv.* **2015**, *5*, 15870.
- 35 Janiak, C. *J. Chem. Soc. Dalton Trans.* **2000**, 3885.
- 36 Pariyar, A.; Stansbery, J.; Patel, R.L.; Liang, X.; Choudhury, A. *J. Coord. Chem.* **2016**, *69*, 1957.
- 37 Köberl, M.; Cokoja, M.; Herrmann, W.A.; Kühn, F.E. *Dalton Trans.* **2011**, *40*, 6834.
- 38 Addison, A.W.; Rao, T.N.; Reedijk, J.; van Rijn, J.; Verschoor, G.C. *J. Chem. Soc., Dalton Trans.* **1984**, 1349.
- 39 Blatov, V.A.; Shevchenko, A.P. TOPOS Professional v. 4.0, Samara State University, Russia.
- 40 Desiraju, G.R.; Steiner, T. *The Weak Hydrogen Bond in Structural Chemistry and Biology*, **1999**, OUP, Oxford.
- 41 Wöll, Ch.; Chiang, S.; Wilson, R.J.; Lippel, P.H. *Phys. Rev. B* **1989**, *39*, 7988.
- 42 Barth, J.V.; Brune, H.; Ertk, G. *Phys. Rev. B* **1990**, *42*, 9307.
- 43 Pham, T.A.; Song, F.; Alberti, M.N.; Nguyen, M.-T.; Trapp, N.; Thilgen, C.; Diederich, F.; Stöhr, M. *Chem. Commun.* **2015**, *51*, 14473.
- 44 Lin, N.; Payer, D.; Dmitriev, A.; Strunskus, T.; Wöll, C.; Barth, J.V.; Kern, K. *Angew. Chem. Int. Ed.* **2005**, *44*, 1488.
- 45 Pawin, G.; Wong, K. L.; Kim, D.; Sun, D.; Bartels, L.; Hong, S.; Rahman, T. S.; Carp, R.; Marsella, M. *Angew. Chem. Int. Ed.* **2008**, *47*, 8442.
- 46 Sirtl, T.; Schlögl, S.; Rastgoo-Lahrood, A.; Jelic, J.; Neogi, S.; Schmittel, M.; Heckl, W.M.; Reuter, K.; Lackinger, M. *J. Am. Chem. Soc.* **2013**, *135*, 691.
- 47 Lin, N.; Payer, D.; Dmitriev, A.; Strunskus, T.; Wöll, C.; Barth, J. V.; Kern, K. *Angew. Chem. Int. Ed.* **2005**, *44*, 1488.
- 48 Wintjes, N.; Hornung, J.; Lobo-Checa, J.; Voigt, T.; Samuely, T.; Thilgen, C.; Stöhr, M.; Diederich, F.; Jung, T.A. *Chem. Eur. J.* **2008**, *14*, 5794.
- 49 Enache, M.; Maggini, L.; Llanes-Pallas, A.; Jung, T. A.; Bonifazi, D.; Stöhr, M. *J. Phys. Chem. C* **2014**, *118*, 15286.



SYNOPSIS TOC

Supplementary information to accompany:

**The different faces of 4'-pyrimidinyl functionalized 4,2':6',4''-terpyridines: metal organic assemblies from solution and on Au(111) and Cu(111) surface platforms**

Thomas Nijs,<sup>a</sup> Y. Maximilian Klein,<sup>b</sup> S. Fatemeh Mousavi,<sup>a</sup> Aisha Ahsan,<sup>a</sup> Sylwia Nowakowska,<sup>a</sup> Edwin C. Constable,<sup>b</sup> Catherine E. Housecroft<sup>b\*</sup> and Thomas Jung<sup>a,c\*</sup>

<sup>a</sup> Department of Physics, University of Basel, Klingelbergstrasse 82, 4056 Basel, Switzerland

<sup>b</sup> Department of Chemistry, University of Basel, BPR 1096, Mattenstrasse 24a 4058 Basel, Switzerland

<sup>c</sup> Laboratory for Micro- and Nanotechnology, Paul Scherrer Institut, 5232 Villigen, Switzerland.

**Supplementary information**

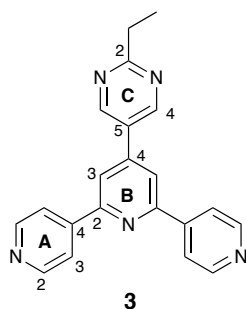
**Experimental section**

**General.** <sup>1</sup>H and <sup>13</sup>C NMR spectra were recorded on a Bruker DRX-500 NMR spectrometer with chemical shifts referenced to residual solvent peaks (TMS =  $\delta$  0 ppm). Electrospray ionisation (ESI) mass spectra were measured on a Bruker esquire 3000plus spectrometer or Shimadzu LCMS-2020 instrument, and high resolution ESI mass spectra on a Bruker maXis 4G QTOF instrument.

Compounds **1** and **2** were prepared as previously reported.<sup>1</sup> Cu(OAc)<sub>2</sub>·H<sub>2</sub>O and Cu<sub>2</sub>(CF<sub>3</sub>SO<sub>3</sub>)<sub>2</sub>·C<sub>7</sub>H<sub>8</sub> were purchased from Sigma Aldrich.

### Compound 3

Structure of **3** with atom labelling for NMR spectroscopic assignments.



2-Ethylpyrimidine-5-carbaldehyde (0.5 g, 3.67 mmol) was dissolved in EtOH (80 mL), and 4-acetylpyridine (0.92 mL, 0.1 g, 8.07 mmol) was added followed by crushed solid KOH (0.52 g, 9.18 mmol). Aqueous NH<sub>3</sub> (25%, 18.1 mL, 117 mmol) was added dropwise and the mixture was stirred for ~15 h at ambient temperature. A white precipitate formed which was separated by filtration, washed with water (3 × 10 mL), EtOH (3 × 10 mL) and Et<sub>2</sub>O (3 × 10 mL). Compound **3** was obtained as a white solid (0.21 g, 3.67 mmol, 16.8 %). M.p. = 275.3 °C. <sup>1</sup>H NMR (500 MHz, CDCl<sub>3</sub>) δ / ppm 9.03 (s, 2H, H<sup>C4</sup>), 8.82 (m, 4H, H<sup>A2</sup>), 8.07 (m, 4H, H<sup>A3</sup>), 8.01 (s, 2H, H<sup>B3</sup>), 3.13 (q, *J* = 7.6 Hz, 2H, H<sup>Et</sup>), 1.45 (t, *J* = 7.6 Hz, 3H, H<sup>Et</sup>). <sup>13</sup>C{<sup>1</sup>H} NMR (126 MHz, CDCl<sub>3</sub>) δ / ppm 173.6 (C<sup>C2</sup>), 156.1 (C<sup>A4</sup>), 155.3 (C<sup>C4</sup>), 150.9 (C<sup>A2</sup>), 145.5 (C<sup>B2</sup>), 145.3 (C<sup>B4</sup>), 128.8 (C<sup>C5</sup>), 121.3 (C<sup>A3</sup>), 118.5 (C<sup>B3</sup>), 32.7 (C<sup>Et</sup>), 12.8 (C<sup>Me</sup>). ESI-MS *m/z* 340.23 [M+H]<sup>+</sup> (calc. 340.16). High resolution ESI-MS *m/z* 340.1561 [M+H]<sup>+</sup> (calc. 340.1557)

### [Cu<sub>2</sub>(OAc)<sub>4</sub>(**3**)]<sub>*n*</sub>

A solution of Cu(OAc)<sub>2</sub>·H<sub>2</sub>O (4.11 mg, 0.021 mmol) in MeOH (8 mL) was layered over a solution of **3** (7.0 mg, 0.021 mmol) in CHCl<sub>3</sub> (5 mL). Blue crystals of [Cu<sub>2</sub>(OAc)<sub>4</sub>(**3**)]<sub>*n*</sub> (0.9 mg, 0.00128 mmol, 12.2 % based on Cu(OAc)<sub>2</sub>) were

obtained after 1–2 weeks. Insufficient amount of material was obtained for bulk sample analysis.

### **$\{[\text{Cu}(\mathbf{3})(\text{OMe})(\text{MeOH})][\text{CF}_3\text{SO}_3]\cdot\text{MeOH}\}_n$**

A solution of  $\text{Cu}_2(\text{CF}_3\text{SO}_3)_2\cdot\text{C}_7\text{H}_8$  (10.7 mg, 0.021 mmol) in MeOH (8 mL) was layered over a solution of **3** (7.0 mg, 0.021 mmol) in  $\text{CHCl}_3$  (5 mL). Blue crystals of  $\{[\text{Cu}(\mathbf{3})(\text{OMe})(\text{MeOH})][\text{CF}_3\text{SO}_3]\cdot\text{MeOH}\}_n$  (5.4 mg, 0.00834 mmol, 39.7% based on **3**) were obtained after 1–2 weeks. The bulk material was characterized by powder diffraction.

**Crystallography.** Single crystal data were collected on a STOE StadiVari diffractometer equipped with a Pilatus300K detector and with a Metaljet D2 source; data reduction, solution and refinement used the programs STOE X-Area, STOE X-RED, SuperFlip and CRYSTALS respectively.<sup>2,3,4</sup> Structure analysis used the programs Mercury v. 3.6<sup>5,6</sup> and TOPOS.<sup>7</sup> Powder diffraction data were collected on a Stoe Stadi P powder diffractometer.

$[\text{Cu}_2(\text{OAc})_4(\mathbf{3})]_n$ .  $\text{C}_{29}\text{H}_{29}\text{Cu}_2\text{N}_5\text{O}_8$ ,  $M = 702.67$ , blue plate, monoclinic, space group  $C2/c$ ,  $a = 26.0869(15)$ ,  $b = 14.8694(9)$ ,  $c = 8.1356(5)$  Å,  $\beta = 108.012(3)^\circ$ ,  $U = 3001.11(18)$  Å<sup>3</sup>,  $Z = 4$ ,  $D_c = 1.555$  Mg m<sup>-3</sup>,  $\mu(\text{Ga-K}\alpha) = 2.248$  mm<sup>-1</sup>,  $T = 123$  K. Total 29718 reflections, 2832 unique,  $R_{\text{int}} = 0.037$ . Refinement of 2686 reflections (236 parameters) with  $I > 2\sigma(I)$  converged at final  $R1 = 0.0495$  ( $R1$  all data = 0.0520),  $wR2 = 0.1250$  ( $wR2$  all data = 0.1261),  $\text{gof} = 1.0222$ . CCDC 1585047.

$\{[\text{Cu}(\mathbf{3})(\text{OMe})(\text{MeOH})][\text{CF}_3\text{SO}_3]\cdot\text{MeOH}\}$ .  $\text{C}_{25}\text{H}_{28}\text{CuF}_3\text{N}_5\text{O}_6\text{S}$ ,  $M = 647.13$ , blue needle, monoclinic, space group  $P2_1/n$ ,  $a = 7.3589(2)$ ,  $b = 19.2305(3)$ ,  $c = 19.2279(4)$  Å,  $\beta = 93.221(2)^\circ$ ,  $U = 2716.74(6)$  Å<sup>3</sup>,  $Z = 4$ ,  $D_c = 1.582$  Mg m<sup>-3</sup>,  $\mu(\text{Ga-}$

$K\alpha$ ) = 5.221 mm<sup>-1</sup>,  $T$  = 123 K. Total 50738 reflections, 5511 unique,  $R_{\text{int}}$  = 0.065. Refinement of 4419 reflections (376 parameters) with  $I > 2\sigma(I)$  converged at final  $R1$  = 0.04705 ( $R1$  all data = 0.0577),  $wR2$  = 0.0976 ( $wR2$  all data = 0.1090),  $\text{gof}$  = 1.0087. CCDC 1585048.

### **On-surface study**

*In-situ* sample preparation, scanning tunneling microscopy (STM) investigations and X-ray photoelectron spectroscopy (XPS) measurements (performed at the Paul Scherrer Institute (PSI), Laboratory for Micro- and Nanotechnology) were carried out under ultrahigh vacuum (UHV) conditions (base pressure of  $5 \times 10^{-11}$  mBar). Au(111) and Cu(111) crystals (MaTeck GmbH) were prepared by subsequent sputtering annealing cycles (Ar<sup>+</sup> ions at 1 keV, 630 K respectively). Molecules were deposited by means of thermal evaporation from a commercial evaporator (Kentax GmbH) with sublimation temperatures of around 480 K. Metal adatoms were added by e-beam evaporator (Oxford Applied research). Quartz crystal microbalance was used to control the coverage. Sample preparation as well as XPS were performed at room temperature, whereas STM images were recorded at 5 K. Typical scanning parameters were 1 V and 10 pA, in constant current mode (Omicron Nanotechnology GmbH). STM tips (90% Pt, 10% Ir) were mechanically cut and sputtered *in-situ* with Ar<sup>+</sup> ions. For XPS, was a monochromatic Al  $K\alpha$  X-ray source with a full width at half maximum (FWHM) of 1.2 eV was used. As analysis software was used WSxM<sup>[8]</sup> in case of STM and Unifit in case of XPS.

## Supplementary Figures

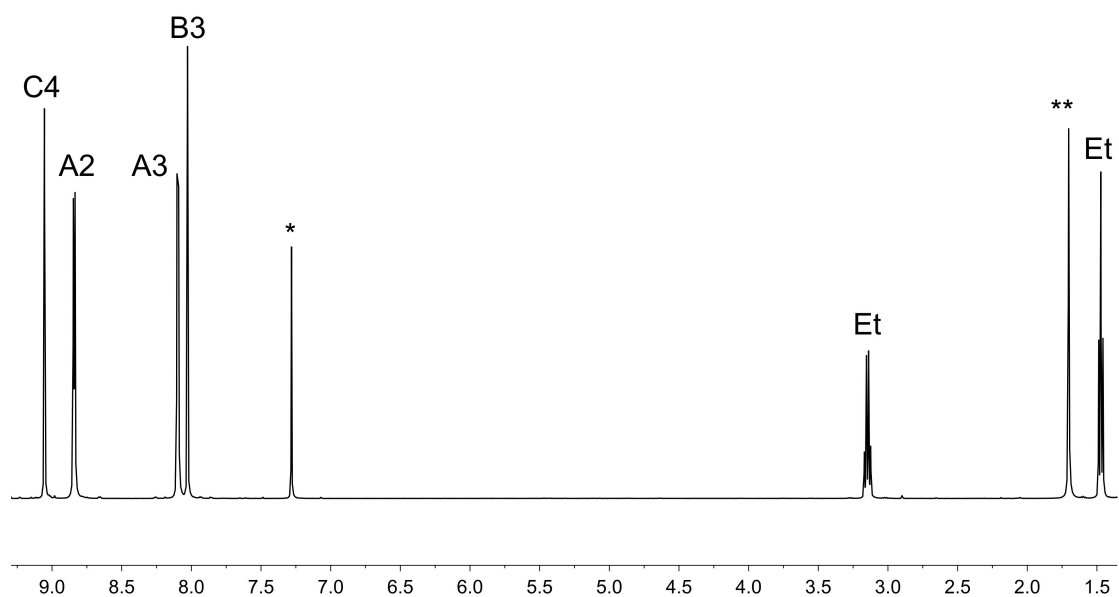


**Fig. S1.** 500 MHz  $^1\text{H}$  NMR spectrum of **3** in  $\text{CDCl}_3$ . \* = residual  $\text{CHCl}_3$ ; \*\* = water.

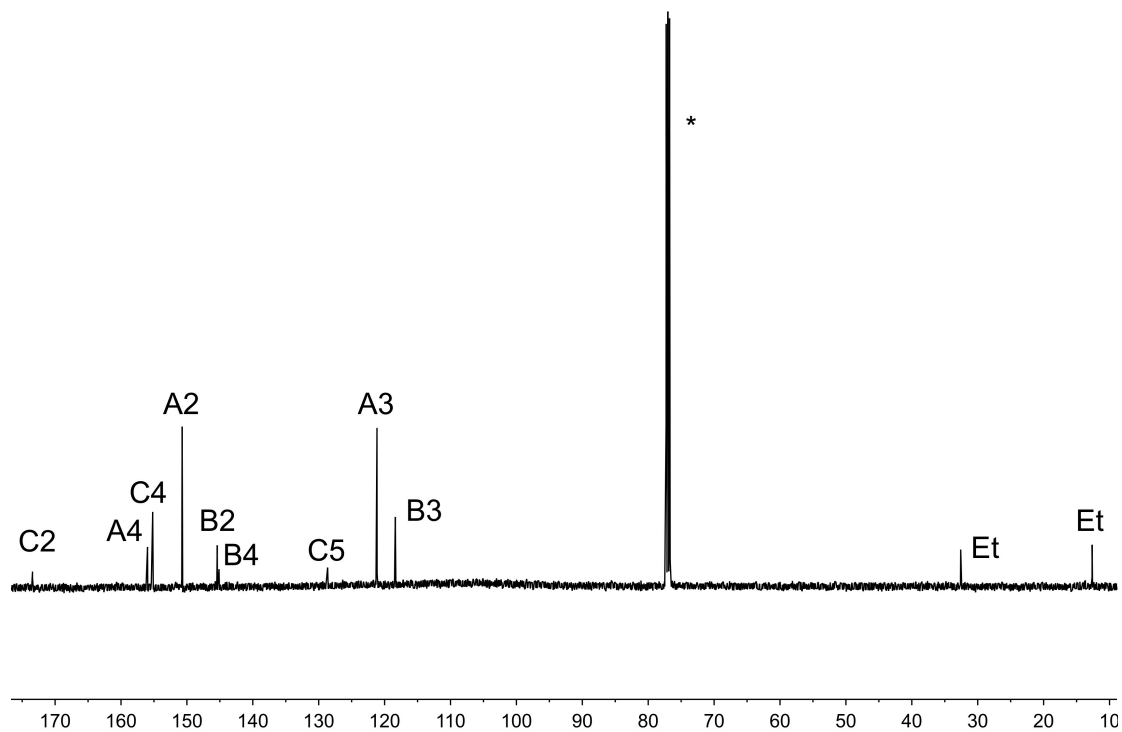


**Fig. S2.** 126 MHz  $^{13}\text{C}$  NMR spectrum of **3** in  $\text{CDCl}_3$ . \* =  $\text{CDCl}_3$ .

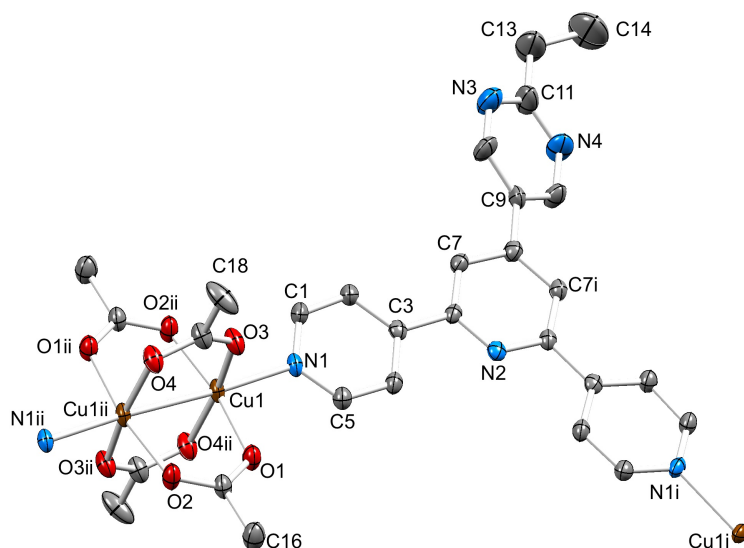


**Fig. S3.** Structure of the repeat unit (with symmetry generated Cu1i and N1ii atoms) in  $[\text{Cu}_2(\text{OAc})_4(\mathbf{3})]_n$  (ellipsoids plotted at 40% probability level and H atoms omitted); the ring containing N3 and N4 is disordered (see text). Symmetry codes:  $i = 1-x, y, 3/2-z$ ;  $ii = 3/2-x, 3/2-y, 1-z$ . Selected bond parameters: Cu1–N1 = 2.141(2), Cu1–O1 = 1.972(2), Cu1–O3 = 1.9750(19), Cu1–O4<sup>ii</sup> = 1.9879(19), Cu1–O2<sup>ii</sup> = 1.967(2), Cu1–Cu1<sup>ii</sup> = 2.6096(7) Å; O4<sup>ii</sup>–Cu1–N1 = 98.87(8), O2<sup>ii</sup>–Cu1–N1 = 95.33(8), O1–Cu1–N1 = 95.67(8), O3–Cu1–N1 = 92.31(8)°.

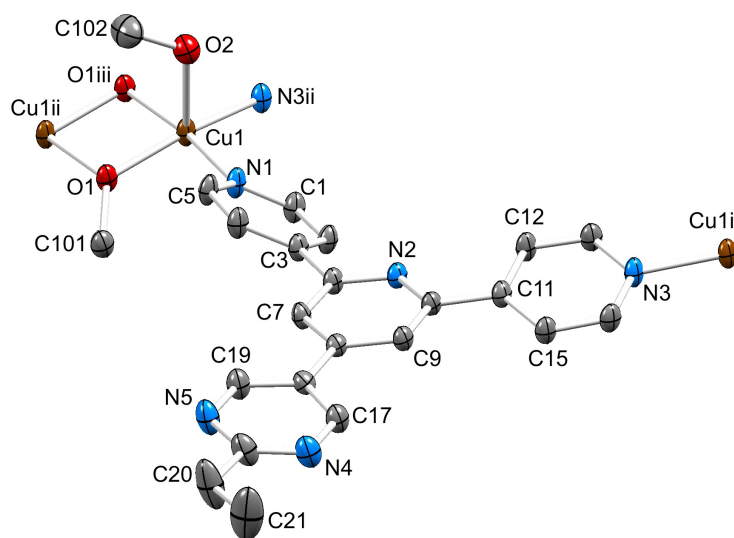


**Fig. S4.** Structure of the repeat unit (with symmetry generated atoms) in  $\{[\text{Cu}(\mathbf{3})(\text{OMe})(\text{MeOH})][\text{CF}_3\text{SO}_3]\cdot\text{MeOH}\}_n$  (ellipsoids plotted at 40% probability level and H atoms omitted). Symmetry codes:  $i = 3/2-x, 1/2+y, 1/2-z$ ;  $ii = 3/2-x, -1/2+y, 1/2-z$ ;  $iii = 2-x, 1-y, -z$ . Selected bond parameters: Cu1–N3<sup>ii</sup> = 2.008(3), Cu1–O1 = 1.944(2), Cu1–O1<sup>iii</sup> = 1.946(2), Cu1–N1 = 2.008(2), Cu1–O2 = 2.301(3), Cu1–Cu1<sup>ii</sup> = 3.0454(8) Å; N1–Cu1–O1 = 93.69(10), N1–Cu1–O2 = 87.27(11), O1–Cu1–O2 = 105.10(10), N3<sup>ii</sup>–Cu1–O1<sup>iii</sup> = 92.67(9), N3<sup>ii</sup>–Cu1–N1 = 97.14(10), O1<sup>iii</sup>–Cu1–O1 = 76.95(9), N3<sup>ii</sup>–Cu1–O2 = 94.15(11), O1<sup>iii</sup>–Cu1–O2 = 92.25(10), N3<sup>ii</sup>–Cu1–O1 = 158.33(11), O1<sup>iii</sup>–Cu1–N1 = 170.18(10)°.

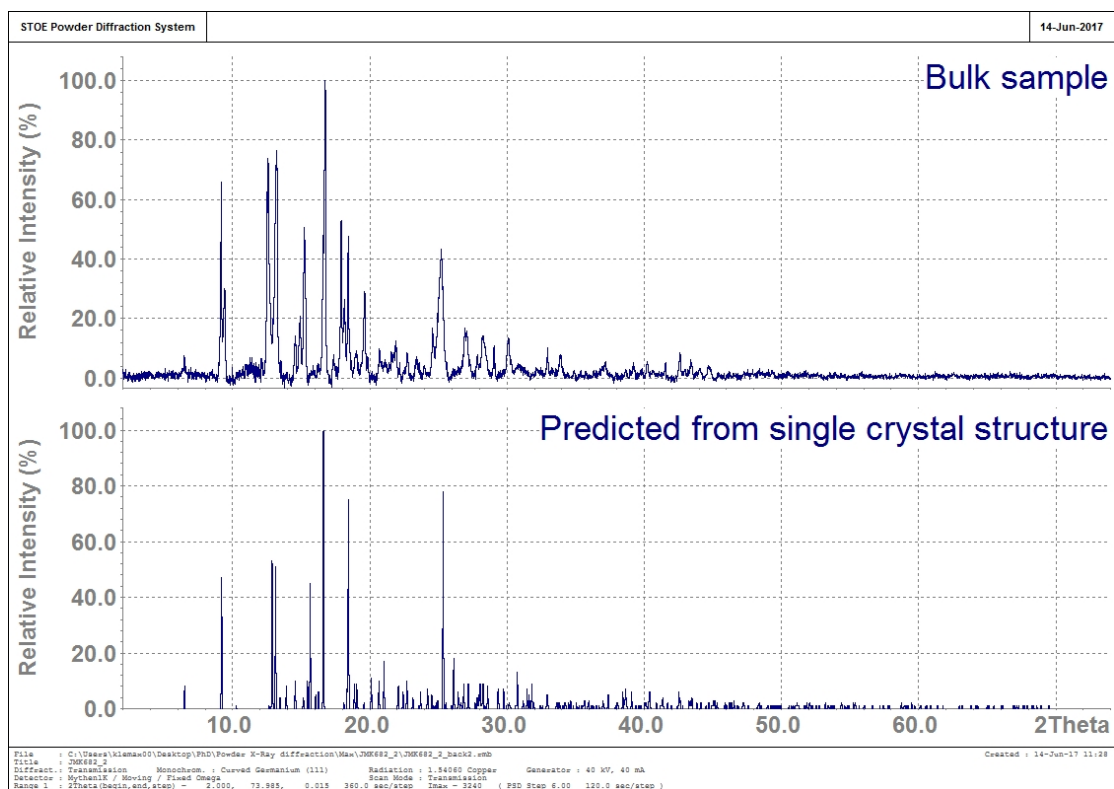


**Fig. S5.** Comparison of the powder diffraction patterns of the bulk sample obtained from the reaction of  $\text{Cu}_2(\text{CF}_3\text{SO}_3)_2$  and **3** (top) and that predicted from the single crystal structure of  $\{[\text{Cu}(\mathbf{3})(\text{OMe})(\text{MeOH})][\text{CF}_3\text{SO}_3]\cdot\text{MeOH}\}_n$  (123 K).

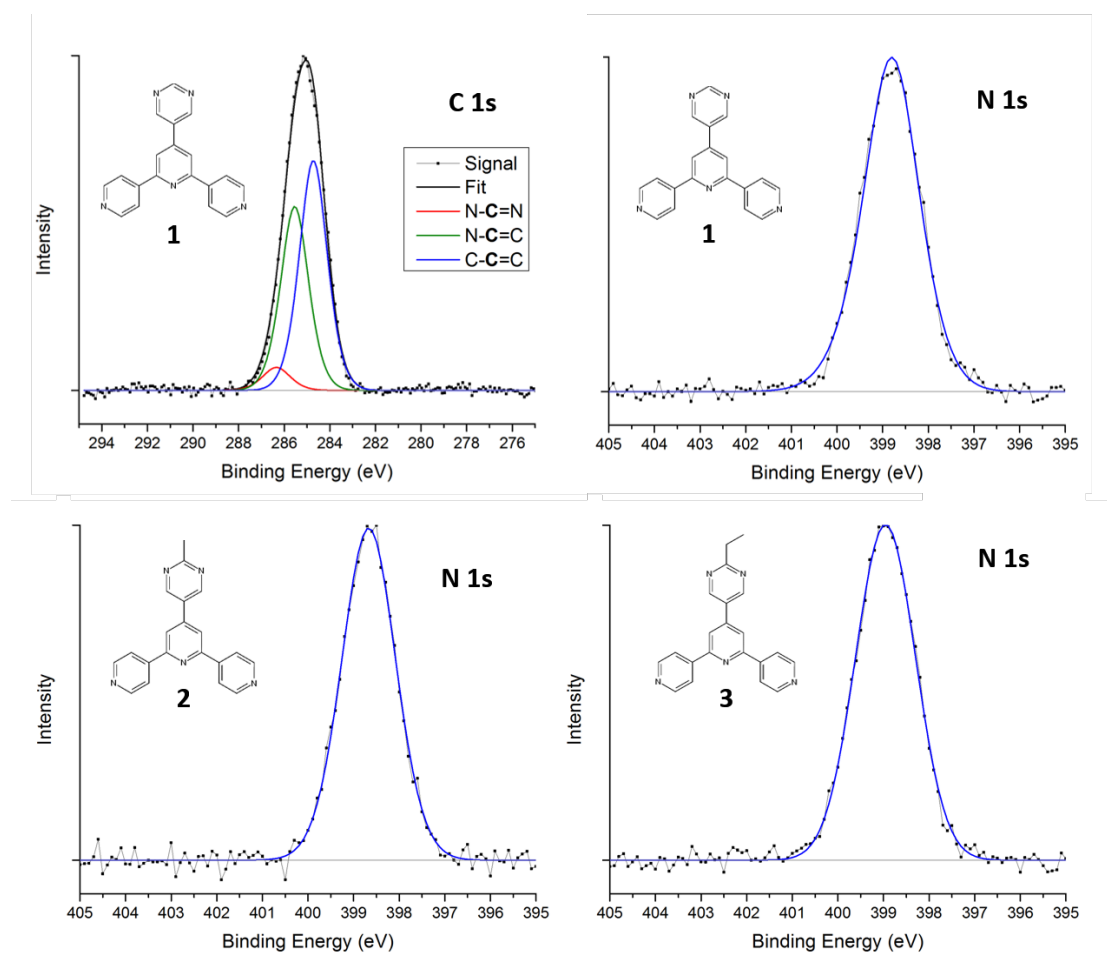


**Fig. S6.** XPS analysis of multilayer of **1**, **2**, **3** on Au(111) indicates sublimation of intact compounds. The C 1s vs. N 1s peak ratio as well as the detailed deconvolution of the C 1s peak provide the correct stoichiometry. The N 1s peak is situated at  $398.8 \pm 0.1$  eV for all 3 compounds, consistent with coordination.

- (1): C:C:C = 1:8:10. Total N:C ratio => 1:3.7. (Example shown)
- (2): C:C:C = 1:8:11. Total N:C ratio => 1:4.0.
- (3): C:C:C = 1:8:12. Total N:C ratio => 1:4.2.

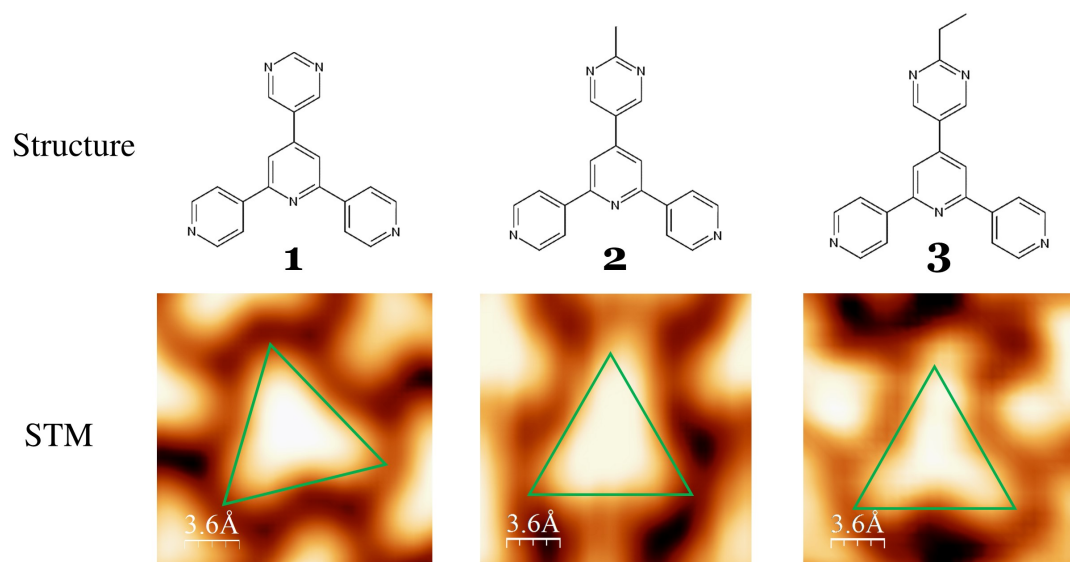


**Fig. S7.** Enlargement of manuscript Fig. 3.

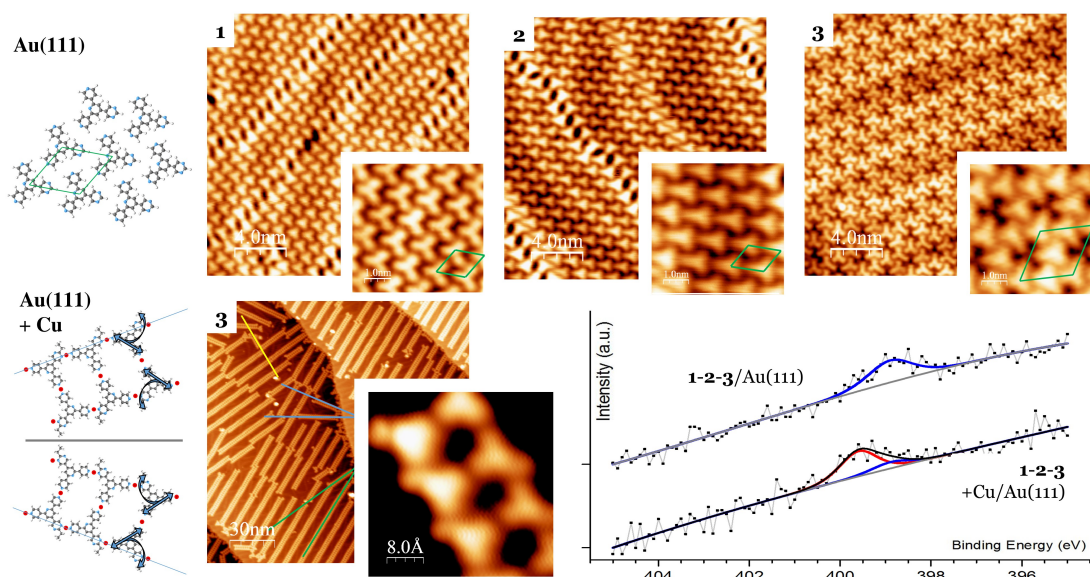


**Fig. S8.** Enlargement of manuscript Fig. 4.

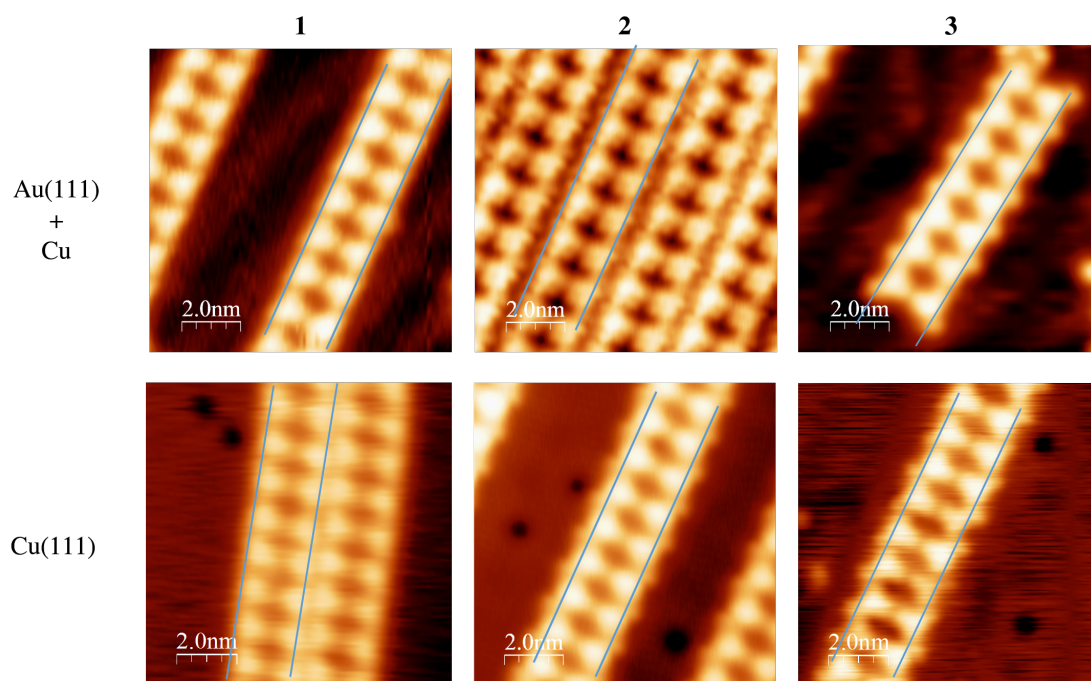


**Fig. S9.** The remarkable similarity between the chains of **1**, **2** and **3** on a) Au(111) + Cu adatoms (top row), b) Cu(111) (bottom row), and c) the chains of same compound on the different substrate (respective columns) is illustrated by drawing two parallel blue lines of 2.3 nm distance on all images, corresponding to the width of all ladders. Ethyl and methyl imaging groups are clearly seen on the outside of the blue lines. Please note: coverage of **2** on Au(111) was high; still chains are separated by a gap due to presence of the functionalization disabling proper stacking. In its absence however, e.g. in case of **1** on Cu, chains always make contact. On Au(111) the herringbone reconstruction is always visible on the substrate terraces; on Cu(111) “etching” spots are always visible.

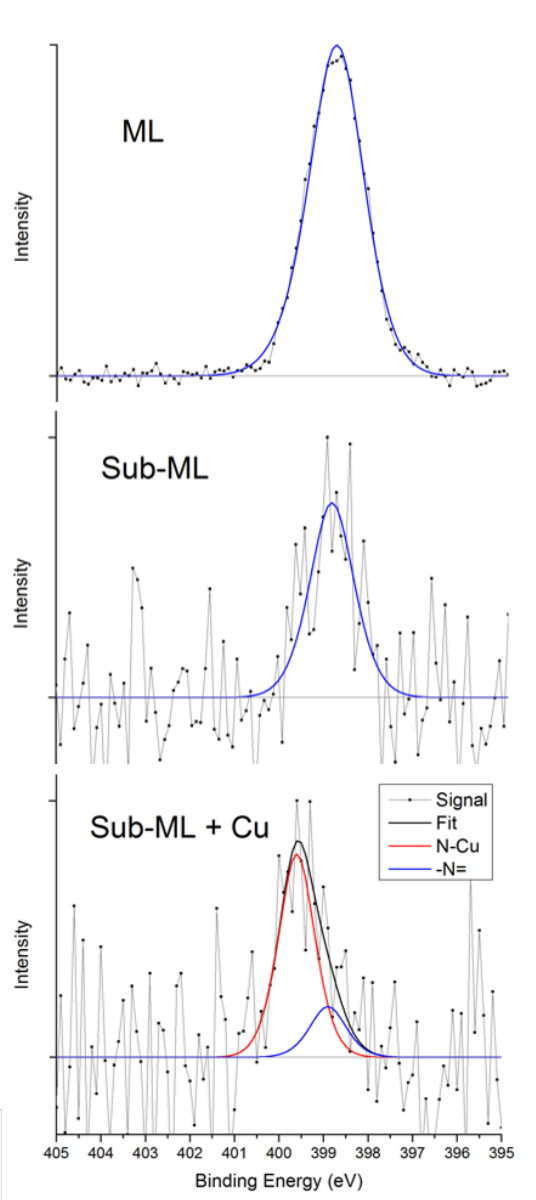


**Fig. S10.** Detailed N 1s peak analysis upon Cu-coordination of compound **1** (representative for all compounds) on Au(111) shows no peak position shift between multilayer and sub-mololayer coverages (probably due to little surface interaction; 398.8 eV). Upon Cu adatom supply at RT, coordination occurs at the four outer nitrogen atoms (new red peak; 399.6 eV). As previously reported, the central tpy nitrogen remains non-coordinated (remaining blue peak)<sup>[9]</sup>, resulting in 4:1 ratio.

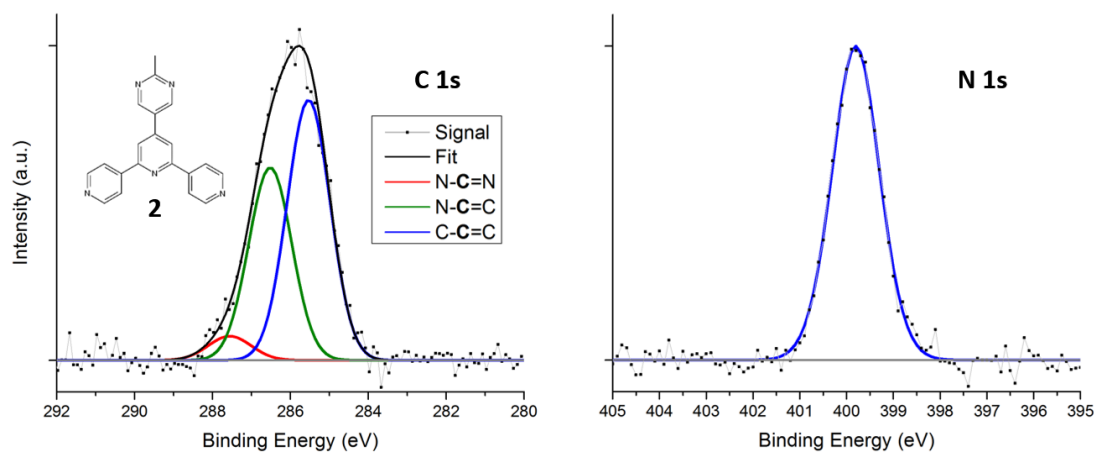


**Fig. S11.** XPS analysis of multilayer of **1**, **2**, **3** on Cu(111) presents similar results as on Au(111). Deconvolution of C 1s peak show correct C:C:C ratios, and all three compounds exhibit same N 1s peak. This is however situated at 399.8 eV. Also, C:N ratio changed from 4:1 to 5:1.

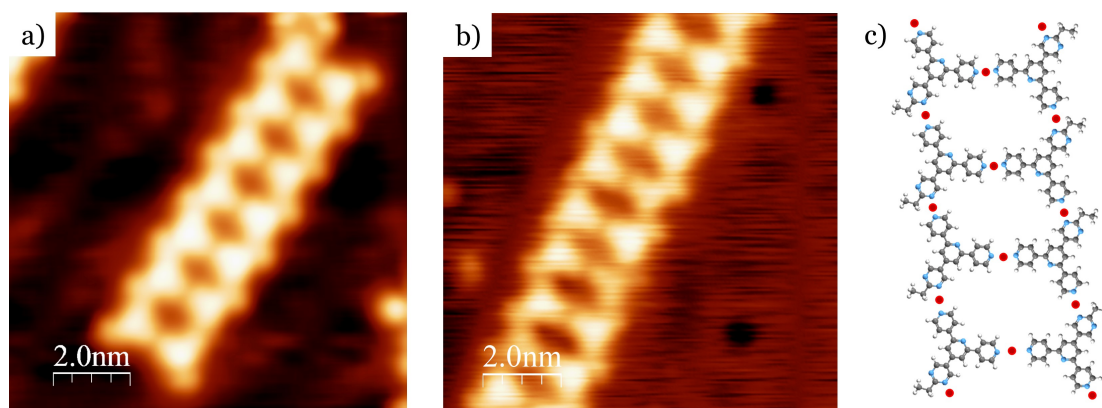


**Fig. S12.** Enlargement of manuscript Fig. 5.

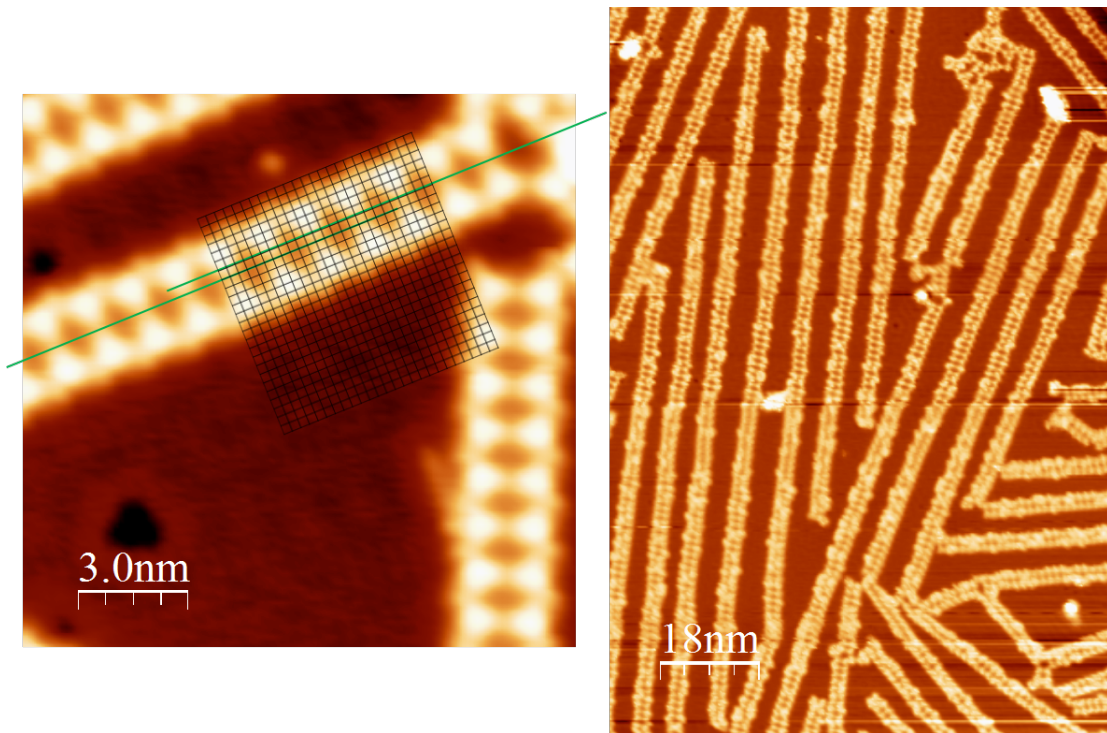


**Fig. S13.** Left: closer analysis of “wiggles” occurring in the chains. The two green lines are adjusted to the straight parts of the chains (middle nodal point as reference). On top a 25x25 grid for more precise measurement, where one box is adjusted to match the distance between the two green lines. This turns out to be 2.56 Å, exactly corresponding to one lattice jump in the Cu substrate. Right: Chains exceed 125 nm of length (please note the presence of Xenon adatoms). Both images were taken on Cu(111) substrate.

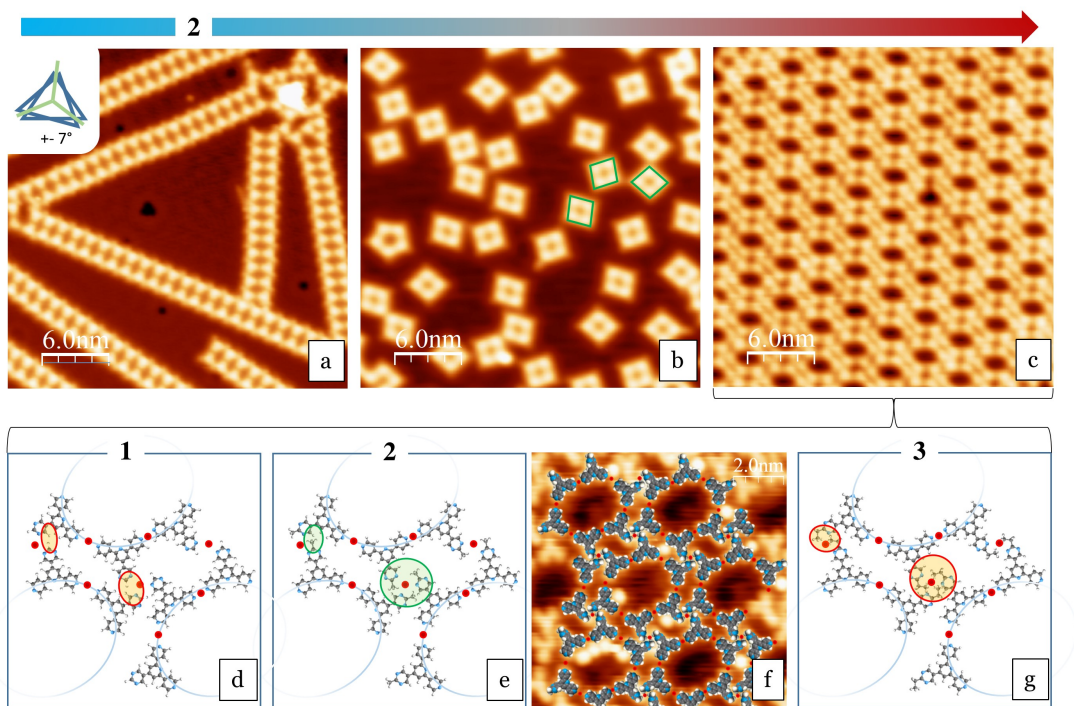


**Fig. S14.** Enlargement of manuscript Fig. 6.

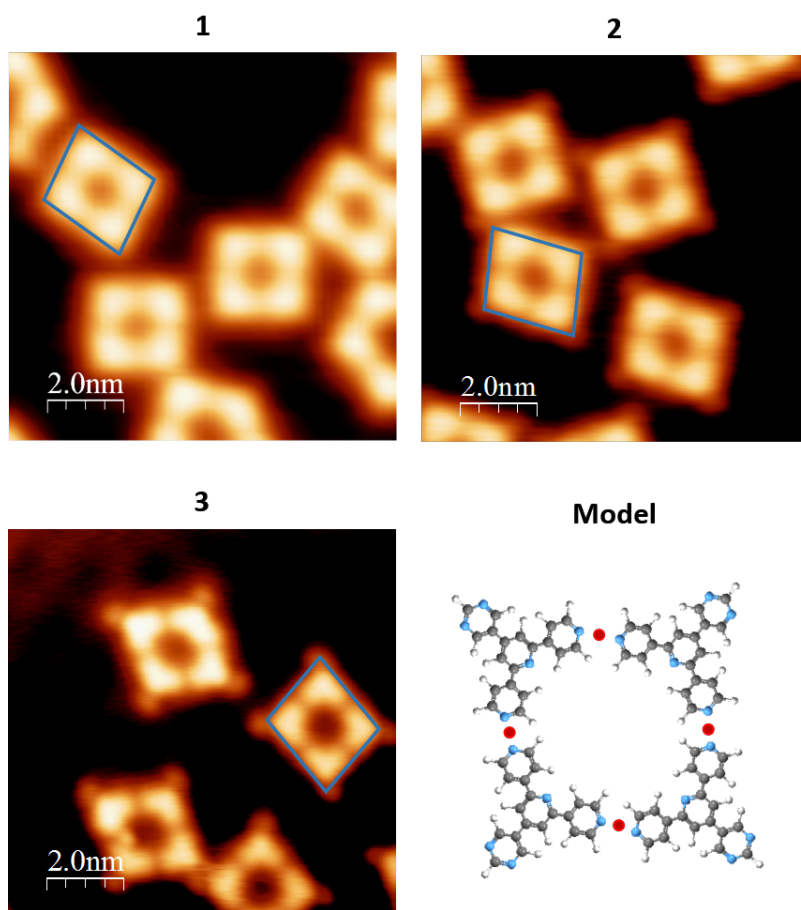


**Fig. S15.** Same blue rhombus of approx. 2.3 nm is drawn on top of tetramers of **1**, **2** and **3** on Cu(111). The as imaging groups acting methyl and ethyl functionalizations are clearly visible in the outside corners of the rhombuses, leaving the core unaltered for all three compounds.

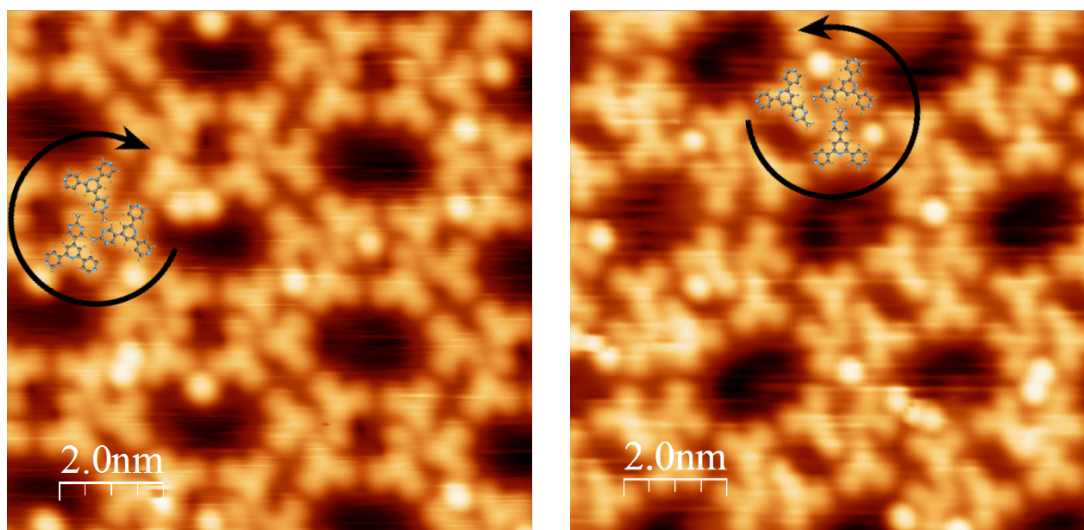


**Fig. S16.** The nanoporous assembly of **2** on Cu(111) is present in both chiralities.

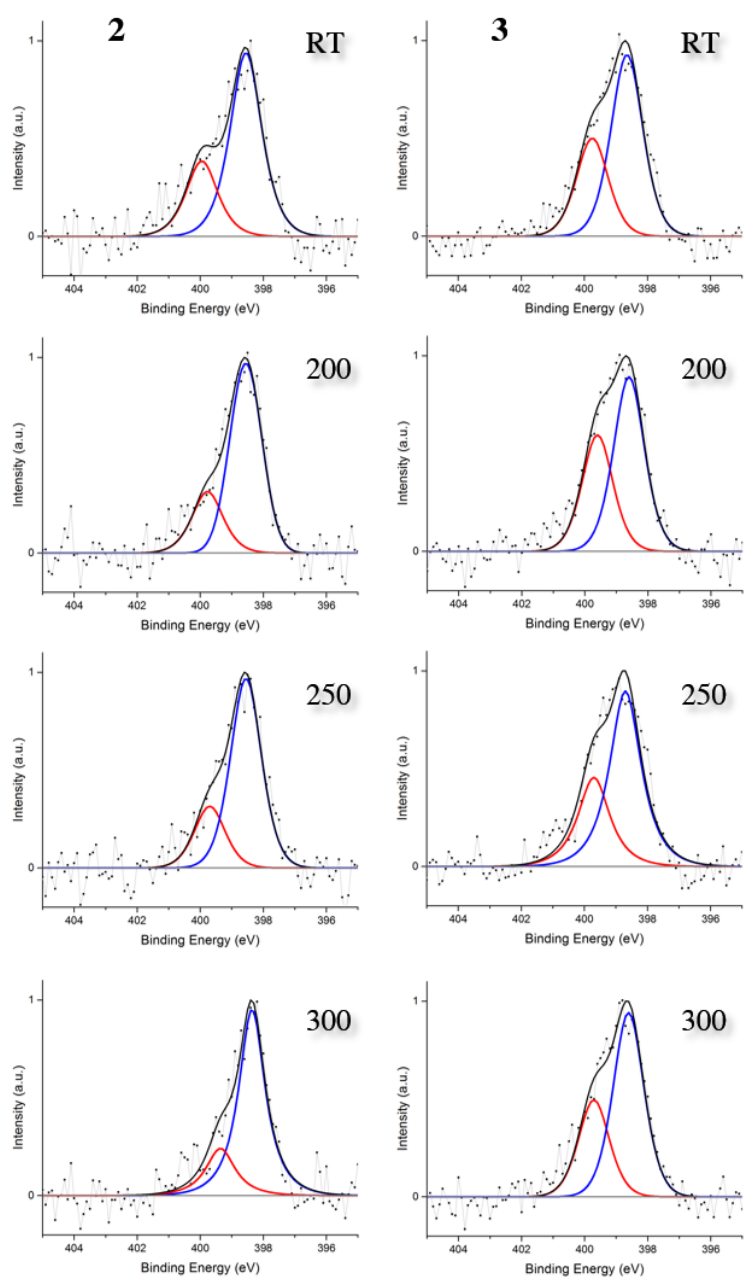


**Fig. S17.** Temperature dependent XPS analysis of **2** (left column) shows no difference, neither during annealing, nor between the different compounds (**3** in right column). Peak positions are 398.6 and 399.7 ( $\pm 0.2$ ) eV in all cases.

**Table S1:** XPS N 1s peak positions of **1,2,3** experimentally obtained:

Molecule/Substrate	-N= [eV]	N-Cu [eV]	
Multilayer <b>1,2,3</b> /Au(111)	398.8	-	
<b>1,2,3</b> /Au(111)	398.8	-	
<b>1,2,3</b> +Cu/Au(111)	398.8	399.6	
Multilayer <b>1,2,3</b> /Cu(111)	399.8	-	
<b>1,2,3</b> /Cu(111)	398.6	398.6	399.7
<b>1,2,3</b> /Cu(111) + Anneal	398.6	398.6	399.7

**Table S2:** Literature comparison of values in Table S1.

Molecule/Substrate	-N= [eV]	N-Cu [eV]
Multilayer <b>1,2,3</b> /Au(111)	398.9 <sup>9</sup>	-
<b>1,2,3</b> +Cu/Au(111)	398,3 <sup>9,10,11</sup> 398.5 <sup>12</sup>	400.2 <sup>10</sup> (Pt) 399.2 <sup>12</sup> (Co) 399.7 <sup>9</sup> (Cu)
Multilayer <b>1,2,3</b> /Cu(111)	399.1 <sup>13,14</sup>	-
<b>1,2,3</b> /Cu(111)	397.8 <sup>15</sup> 398.3 <sup>13,14</sup> 398.8 <sup>17</sup>	398.2 <sup>16</sup> 398.2 <sup>14</sup> 398.9 <sup>17</sup>

Au(111):

- Similar peak position for multilayer as sub-monolayer as a result of no strong interaction of the compounds with the substrate.
- Major N 1s peak shift to higher binding energies upon coordination.<sup>9,10,12</sup>

Cu(111):

- Due to extra-atomic relaxation effect, multilayer N 1s peak is positioned at a higher binding energy than sub-monolayer N 1s peak.<sup>13,14,18</sup>
- Upon coordination, no major peak position change has been detected between non-coordinated and coordinated pyridylic N.<sup>14,17</sup>
- The second prominent and independent peak at higher binding energy cannot be neglected nor attributed to the shakeup process explained in references 11 and 12. Neither does it represent the coordinated nitrogen atoms -- we have reported examples of such non-fitting intra-atomic peak ratios in the past, especially of N 1s on Cu substrates,<sup>19</sup> but not to this extent; also is our current result in accordance to literature. The solution seems to lie in the nature of pyrimidine on Cu(111) surface, since the N 1s peak of 1,3,8,10-tetraazaperopyrene also exhibits an unexplainable additional peak on the higher binding energy, looking very similar to the result presented here (Figure B.3 in ref 15).

- 
1. Klein, Y.M.; Constable, E.C.; Housecroft, C.E.; Zampese, J.A. *Polyhedron* **2014**, *81*, 98.
  2. Stoe & Cie 2011; X-area Software. Stoe & Cie 1996; XRED V1.08.
  3. Palatinus, L.; Chapuis, G. *J. Appl. Cryst.* **2007**, *40*, 786.
  4. Betteridge, P.W.; Carruthers, J.R.; Cooper, R.I.; Prout, K.; Watkin, D.J. *J. Appl. Cryst.* **2003**, *36*, 1487.
  5. Bruno, I.J.; Cole, J.C.; Edgington, P.R.; Kessler, M.K.; Macrae, C.F.; McCabe, P.; Pearson, J.; Taylor, R. *Acta Cryst. B* **2002**, *58*, 389.
  6. Macrae, C.F.; Bruno, I.J.; Chisholm, J.A.; Edgington, P.R.; McCabe, P.; Pidcock, E.; Rodriguez-Monge, L.; Taylor, R.; van de Streek, J.; Wood, P.A. *J. Appl. Cryst.* **2008**, *41*, 466.
  7. Blatov, V.A.; Shevchenko, A.P.; TOPOS Professional v. 4.0, Samara State University, Russia.
  8. Horcas, I.; Fernandez, R.; Gomez-Rodriguez, J.M.; Colchero, J.; Gomez-Herrero, J.; Baro, A.M. *Rev. Sci. Instrum.* **2007**, *78*, 013705.
  9. Nijs, T.; Malzner, F.J.; Fatayer, S.; Wäckerlin, A.; Nowakowska, S.; Constable, E.C.; Housecroft, C.E.; Jung, T.A. *Chem. Commun.* **2015**, *51*, 12297.
  10. Skomski, D.; Tempas, C.D.; Smith, K.A.; Tait, S.L.J. *Am. Chem. Soc.* **2014**, *136*, 9861.
  11. Li, Y.; Xiao, J.; Shubina, T.E.; Chen, M.; Shi, Z.; Schmid, M.; Steinrück, H.P.; Gottfried, J.M.; Lin, N. *J. Am. Chem. Soc.* **2012**, *134*, 6401.
  12. Mette, G.; Sutter, D.; Gurdal, Y.; Schnidrig, S.; Probst, B.; Iannuzzi, M.; Hutter, J.; Albertob, R.; Osterwalder, J. *Nanoscale* **2016**, *8*, 7958.
  13. Lin, Y.P.; Ourdjini, O.; Giovanelli, L.; Clair, S.; Faury, T.; Ksari, Y.; Themlin, J.M.; Porte L.; Abel, M. *J. Phys. Chem. C* **2013**, *117*, 9895.
  14. Klappenberger, F.; Weber-Bargioni, A.; Auwärter, W.; Marschall, M.; Schiffrin, A.; Barth, J.V. *J. Chem. Phys.* **2008**, *129*, 214702.
  15. Matena, M.; Observing cooperative behavior with molecular surface structures, Dissertation, University of Basel 2009.
  16. Matena, M.; Riehm, T.; Stöhr, M.; Jung, T.A. Gade, L.H.; *Angew. Chem. Int. Ed.* **2008**, *47*, 2414.
  17. Li, J.; Wäckerlin, C.; Schnidrig, S.; Joliat, E.; Alberto, E.; Ernst, K.H. *Helv. Chim. Acta* **2017**, *100*, e1600278.
  18. Kohiki, S.; Oki, K.; Konishi, F. *Anal. Sci.* **1985**, *1*, 115
  19. Shchyrba, A.; Wäckerlin, C.; Nowakowski, J.; Nowakowska, S.; Björk, J.; Fatayer, S.; Girovsky, J.; Nijs, T.; Martens, S.C.; Kleibert, A.; Stöhr, M.; Ballav, N.; Jung, T.A.; Gade, L.H. *J. Am. Chem. Soc.* **2014**, *136*, 9355.